CHAPTER 2

Microreactors with Electrical Fields

Anıl Ağıral and **Han J.G.E. Gardeniers***

Contents

Abstract

The use of electric fields in chemistry is considered an important concept of process intensification. The combination of electricity with chemistry becomes particularly valuable at smaller scales, as they are exploited in microreaction technology. Microreactor systems with integrated electrodes provide excellent platforms to

Mesoscale Chemical Systems, MESA + Institute for Nanotechnology, University of Twente, 7500 AE Enschede, The Netherlands

* Corresponding author.
E-mail: j.g.e.gardeniers@utwente.nl

Advances in Chemical Engineering, Volume 38
ISSN: 0065-2377, DOI 10.1016/S0065-2377(10)38002-1

investigate and exploit electric principles as a means to control, activate, or modify chemical reactions, but also preparative separations. One example which is discussed in detail in this chapter is a microplasma, which allows chemistry at moderate temperatures with species which have a reactivity comparable to that at very high temperatures, with potential advantages in energy efficiency. Another highlighted topic is electrokinetic control of chemical reactions, which requires the small scale to operate efficiently. Electrokinetic concepts can be used to control fluid flow, but also to transport or trap particles and molecules. Several less known concepts like electric wind, electric swing adsorption, electrospray, and pulsed electric fields, are discussed, as well as examples of their application. Novel principles to control adsorption and desorption, as well as activity and orientation of adsorbed molecules are described, and the relevance of these principles for the development of new reactor concepts and new chemistry are discussed.

1. INTRODUCTION

1.1 Where chemistry meets electricity

The combination of chemistry and electricity is best known in the form of *electrochemistry*, in which chemical reactions take place in a solution in contact with electrodes that together constitute an electrical circuit. Electrochemistry involves the transfer of electrons between an electrode and the electrolyte or species in solution. It has been in use for the storage of electrical energy (in a galvanic cell or battery), the generation of electrical energy (in fuel cells), the analysis of species in solution (in pH glass electrodes or in ion-selective electrodes), or the synthesis of species from solution (in electrolysis cells).

However, there are many other options to combine electricity with chemistry. One that has been studied intensively for a variety of different applications is *plasma chemistry* (see Fridman, 2008 for a recent overview). A plasma is a partially ionized gas, in which a certain percentage of the electrons is free instead of bound to an atom or molecule. Because the charge neutrality of a plasma requires that plasma currents close on themselves in electric circuits, a plasma reactor shows resemblance to an electrochemical cell, although due to the much lower ionization degree and conductivity, a plasma discharge will typically be operated in the range of hundreds of volts, compared to a few volts in the case of an aqueous electrochemical cell.

An increasing number of industrial and commercial examples of plasma technology exist. Typical *low-pressure* discharge examples are certain types of light sources, including plasma display panels, and microfabrication processes for integrated circuit manufacturing, like sputtering, reactive ion etching and plasma-enhanced chemical vapor

deposition (CVD). Arc discharges, in which a high power thermal discharge of very high temperature (~10,000 K) is generated, are typical examples of *atmospheric pressure* plasmas. Arc discharges are applied in metallurgical processing and welding. Another example of atmospheric plasma is a corona discharge, which is a non-thermal discharge generated by the application of a high voltage to sharp electrode tips. This discharge is used in ozone generators and particle precipitators.

Of particular interest is a dielectric barrier discharge (DBD). This is a nonthermal atmospheric pressure discharge generated by the application of high voltages, in which an *insulator coating* prevents the transition of the plasma discharge into an arc. The process uses a high voltage alternating at kHz to GHz frequencies. Operation at atmospheric pressure is made possible by *a small gap between the electrodes*, from 0.1 mm in plasma displays and 1 mm in ozone generators to several cm in CO_2 lasers. Thus, although DBD is applied at large scale, for example, in the surface functionalization of synthetic fabrics and plastics to improve adhesion of paints and glues (Leroux, 2006, 2008), due to the small gap required it is typically performed in *microsystems*. Furthermore, DBD, besides the possibility to work without the vacuum which is needed for most other plasma processes, operates at *low gas temperatures*, which is the reason why it has become a relevant technique for synthetic purposes. Chemistry in *microplasma devices* will be the main topic elaborated in this chapter.

The above combinations of electricity with chemistry deal with the generation of charged species in either a gas of a liquid medium. This requires ionization, which occurs by electron transfer and transport of charged species in a closed electrical circuit. The charged species themselves, or the radicals generated by them (e.g., radicals generated by electron impact in the gas phase, in a plasma) can be used as activated species taking part in chemical reactions.

On the other hand, one may also use the charges to *enhance mass transport*, either by transporting the chemical species themselves (if they carry a charge), or by transporting the medium in which the chemical species are contained. This *electrokinetic transport* exists in different forms: *electrophoresis* is the movement of charged particles in an electric field due to an electrostatic Coulomb force which drags them through the medium toward an oppositely charged surface, *electroosmosis* is the motion of a polar liquid along charged surfaces under the influence of an electric field, and *dielectrophoresis* (DEP) is based on a force exerted on a (not necessarily charged) dielectric particle subjected to a non-uniform electric field. *Electrowetting-on-dielectric*, or EWOD, can be used to induce a flow of liquid droplets on a surface or in a channel, where the droplets are pulled toward the region with high electric field. All these

electrokinetic principles work best in microsystems, and will be discussed in this chapter for cases in which they are combined with synthetic chemistry.

Finally, one may use charging or polarization of *surfaces*, induced by external electric fields, to control the adsorption and desorption of molecules and the state of these adsorbed molecules, in order to control their chemical reactivity. This is an upcoming field that has not yet been explored to its fullest potential. It involves aspects of *nanotechnology* and *nanoscience*, like the fabrication of structures of several nanometers and stimuli generated by scanning tunneling microscopic probes. The outcome of the research in this field is generally of a fundamental nature. The topic of electronic control of reactions at surfaces will be discussed in the last section of this chapter.

1.2 When chemistry and electricity meet in a narrow alley

The advantages of *microreaction technology* and its establishment as a concept of process intensification have been highlighted many times before in literature, and instead of repeating that matter here, we would like to refer the reader to the many excellent reviews and monographs that have appeared over the last decade (Hessel et al., 2004, 2009; Jähnisch et al., 2004; Jensen, 2001; Kolb et al., 2007; Yoshida, 2008). In cases where microreaction technology involves electricity as a mechanism of activation or manipulation of chemical species (the use of electric fields in chemistry on its own is already considered a valuable process intensification concept, see Stankiewicz and Moulijn, 2000), the advantages of the small scale lie mainly in the shorter distances for mass transport or in the smaller gaps over which electrical fields can be applied. A typical example is, as mentioned before, a microplasma device, in which the small electrode gap allows atmospheric plasma chemistry, which is a result of the fact that although the lifetime of electrons in the gap space is limited because of the dense gas, they still live long enough to excite a significant amount of species. In addition to that, a small gap allows the use of lower voltages to obtain the same electric field strength. Other advantages of the combination of microreaction technology with electrical fields are the large surface-to-volume ratio and the possibility to integrate electrodes at relevant positions in the microreactor device.

In this chapter the focus will be on the application of electrical fields in microreactors, and the potential of such systems for chemical synthesis will be outlined. The end of the chapter will give an overview of less-studied concepts, like electronic control of surface chemistry, and will discuss the opportunities offered by nanotechnology for achieving such control.

2. MICROPLASMA REACTORS

2.1 Atmospheric pressure microplasmas

The plasma state is referred to as the fourth state of matter. It is used to describe a partially or completely ionized gas consisting of positive and negative ions, electrons, and excited and neutral species. The ionization degree of plasma can vary from partially ionized to fully ionized. Plasma exhibits quasineutrality which is referred to as a balance of positive and negative charges. Local charges can be balanced by electrostatic forces which restore the quasineutrality. Plasmas are classified by the number density (particles cm^{-3}) and average kinetic energy (eV), mostly expressed in terms of temperature (K), of the different charged species. The average kinetic energy of electrons, ions, and excited and neutral species depends on the plasma conditions. In equilibrium or thermal plasmas, all constituents (ions, electrons, and neutrals) have the same average temperature, which can vary from a few thousand Kelvin (e.g., in plasma torches) to a few million Kelvin (in fusion plasmas). In a nonthermal low-temperature plasma, the temperature of the ions and neutral species can be close to ambient temperature, while in that same plasma the temperature of the electrons can exceed several thousand Kelvin. The temperature of plasma components (e.g., electrons and species in an excited state) can exceed the temperatures applied in conventional thermal chemical processes and these exceptional conditions of the plasma can generate a thermodynamic nonequilibrium state with a high concentration of energetic and reactive species (Lieberman and Lichtenberg, 1994; Raizer, 1991; von Engel, 1955).

Atmospheric pressure nonthermal discharges may become of great importance for chemical industry because they create a highly reactive environment at cold temperatures and therewith open up alternative, highly flexible, environmentally friendly, and energy-saving processing routes. Characteristics and properties of nonequilibrium atmospheric pressure plasmas can be found in many review articles and books (Becker et al., 2004, 2005, 2006; Foest et al., 2006; Lieberman and Lichtenberg, 1994; Raizer, 1991; Tachibana, 2006; von Engel, 1955).

Atmospheric pressure plasmas, just like most other plasmas, are generated by a high electric field in a gas volume. The few free electrons which are always present in the gas, due to, for example, cosmic radiation or radioactive decay of certain isotopes, will, after a critical electric field strength has been exceeded, develop an avalanche with ionization and excitation of species. Energy gained by the hot electrons is efficiently transferred and used in the excitation and dissociation of gas molecules. In a nonequilibrium atmospheric pressure plasma, collisions and radiative processes are dominated by energy transfer by stepwise processes and three-body collisions. The dominance of these processes has allowed many

novel applications, for example, in medical sterilization, biological decontamination, remediation of pollutants, excimer lamps, and light sources (Foest et al., 2006). However, high-pressure plasmas have a tendency to become unstable due to the rapid transition to arcs and filamentation. To avoid instability problems and maintain a self-sustaining discharge for practical applications, a solution was found in the confinement of the high-pressure plasma to *dimensions below about 1 mm*. Such a plasma is often referred to as a *microplasma*. The current and energy density in this type of plasma is found to be high and results in effective gas heating and momentum transfer from electrons to gas molecules.

Chemistry in reactors with dimensions below 1 mm leads us into the field of *microreactors*. Implementation of microplasmas in microreactors offers the potential to exploit the advantages of atmospheric pressure nonequilibrium chemical processes for efficient synthesis of valuable chemicals and nanostructures as well as the decomposition of hazardous compounds. As mentioned before, microplasmas can be generated at low gas temperatures and possess an electron energy distribution containing large fractions of high-energy electrons, and reactive species deriving from these electrons. In addition, the increased surface area-to-volume ratio in microreactor channels leads to enhanced plasma–surface interactions, which is very useful in cases where active coatings are present on the channel walls. The combination of the reactive species and the additional plasma activation of the surface may be exploited to produce chemical products in an energy efficient manner.

A number of configurations of microplasma reactors will be described here. Classification will be based on the power sources, the electric field switching frequency ranging from DC to GHz, and electrode geometries and materials, extending from DBDs to micro hollow cathodes and microcavity discharges.

2.1.1 DC glow discharges

Atmospheric pressure DC glow discharges can be generated between two electrodes when the current through the discharge is limited to low values by a large resistor (Grotrian, 1915). The microplasma can be stabilized when the electrode separation is kept below 1 mm and the transition to an unstable arc discharge can be avoided when the spatial dimensions of the discharge are kept small enough (Staack et al., 2005). Figure 1 shows a picture of such a discharge in air. Spectroscopic temperature measurements show that the discharge is nonthermal with a gas temperature above room temperature. The nonequilibrium nature of glow discharges for small dimensions may find applications in microreactors for gas reforming, material deposition and the destruction of environmentally harmful substances.

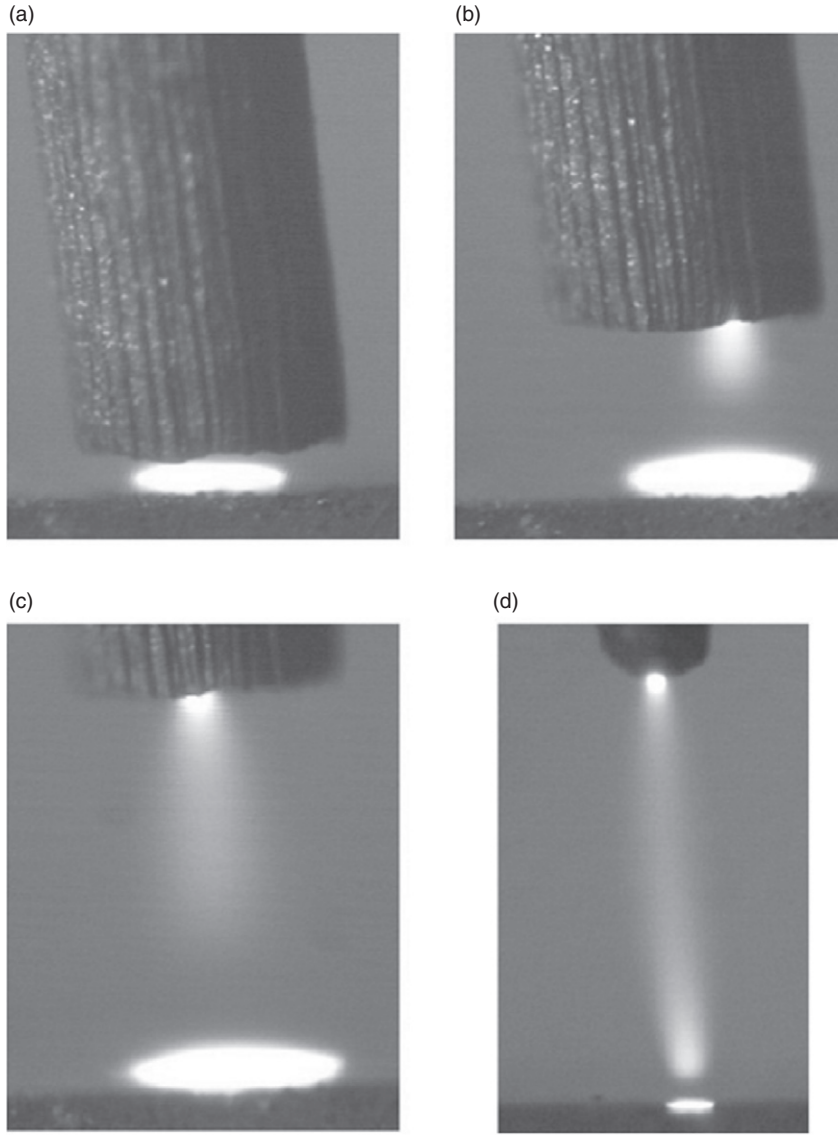

Figure 1 Glow discharges at atmospheric pressure in air at (a) 0.1 mm, (b) 0.5 mm, (c) 1 mm, and (d) 3 mm electrode spacing (Staack et al., 2005; reproduced with permission).

2.1.2 Dielectric barrier discharges

DBDs are nonequilibrium plasmas at atmospheric pressure with applications in ozone generation, surface modification, pollution control, excimer lamps, and recently also in flat plasma display panels (Kogelschatz, 2003). Typical planar DBD configurations are shown in Figure 2. They have at

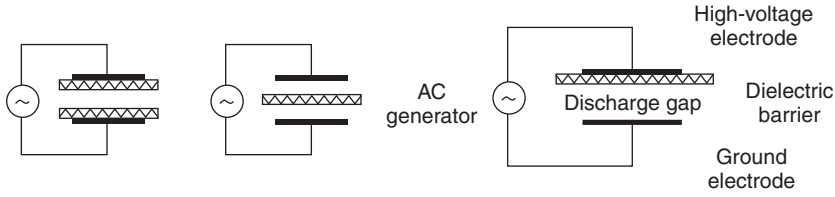

Figure 2 DBD configurations (Kogelschatz, 2003; reproduced with permission).

least one dielectric layer, being an insulator, between electrode and plasma, to prevent arc formation. Dielectric barriers can be glass, ceramic, or polymer coatings. In a DBD configuration, the plasma has a capacitive nature and consists of a large number of microdischarges in the gap between the insulator and the opposite (often uncovered) electrode, where the duration of the filamentary microdischarges is limited to a few nanoseconds (Kogelschatz, 2002). In this way, excess gas heating is minimized, although activation of molecules and atoms in the gas volume is ensured by high-energy electrons created in the microdischarges. The incorporation of a DBD in a microreactor as a miniature source of ions, excited species and radicals can generate a highly reactive and quenching environment which is difficult to obtain in thermochemical processes.

2.1.3 Micro hollow cathode discharges

Micro hollow cathode discharges (MHCDs) were first reported as stable atmospheric pressure microdischarges in cylindrical hollow cathode geometry (Schoenbach, 1996). In a typical hollow cathode structure, there is a cylindrical hole in the cathode, with a ring-shaped anode separated by an insulator (Figure 3a), or a cylindrical opening in a thin solid cathode layer (Figure 3b) (Schoenbach et al., 2003). Because of the relatively simple fabrication process of these electrode configurations, manufacturing of large area arrays of microplasma devices with parallel operation becomes feasible. Flowing gas through the plasma volume inside the hollow part allows the use of these discharges as microreactors. It is also possible to apply a third electrode placed at the anode side to achieve a stable glow discharge with dimensions of up to centimeters in

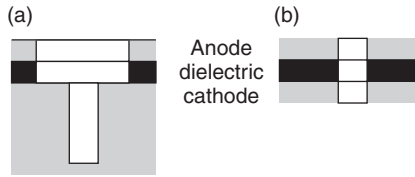

Figure 3 Electrode geometries for MHCDs (Schoenbach et al., 1996; reproduced with permission).

atmospheric pressure (Stark and Schoenbach, 1999). MHCDs can be operated at atmospheric pressure in direct current or pulsed mode with electron densities exceeding those in other nonequilibrium high-pressure glow discharges. Extreme power densities (on the order of $10^5\,W\,cm^{-3}$) make these microdischarges very attractive in microreactors for the efficient decomposition of molecules, such as hydrocarbons and ammonia.

2.1.4 Microcavity discharges

Microcavity plasma devices have cavities with precisely controlled cross sections. Large arrays of these devices have been fabricated in different materials such as ceramics (Allmen et al., 2003), photodefinable glass (Kim and Eden, 2005), alumina structures (Park et al., 2005), and plastic substrates (Anderson et al., 2008). An example with inverted square pyramid microcavities fabricated in silicon is represented in Figure 4. Physical and chemical isolation between the electrodes and the discharge is maintained by the dielectric. The advantage of using silicon as the host material in these microplasma devices is the wide range of microfabrication techniques which are available for this material, which allows production of large arrays of microcavity discharge devices at reasonable expense. As an application example, parallel linear arrays of interconnected cylindrical microcavity plasma elements integrated in microreactors, based on disposable plastic substrates, have been demonstrated (Anderson et al., 2008).

2.1.5 Field emission from tip electrodes

The conditions for gas breakdown in an electrical field can be described in terms of the breakdown voltage as a function of the product of pressure and gap spacing. The resulting graph is known as the Paschen curve

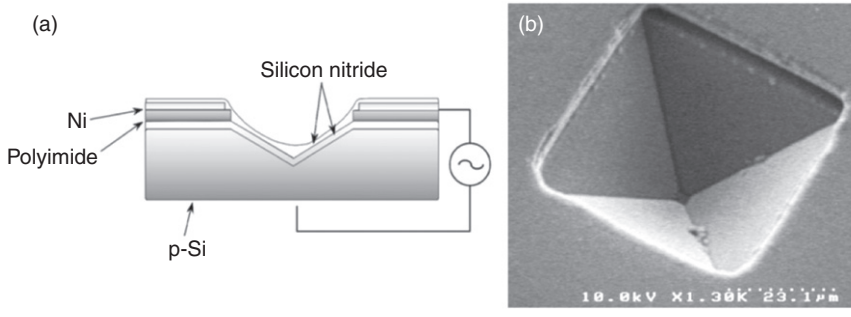

Figure 4 (a) Cross-sectional diagram of a silicon-based microcavity discharge device with an inverted square pyramid microcavity and (b) an SEM (scanning electron microscopy) image of a single microplasma device with $50 \times 50\,\mu m^2$ emitting aperture (Becker et al., 2006; reproduced with permission).

(Paschen, 1889). Breakdown occurs when ions in the gas are accelerated across the gap so that a Townsend avalanche results (Townsend, 1925). For gaps greater than ~10 μm, breakdown has been well studied and occurs when the electric field becomes higher than ~3 V μm^{-1}. However, for air at atmospheric pressure an increase in breakdown voltage was observed for a gap spacing below ~5 μm (Schaffert, 1975). Under these conditions, electrons can tunnel through the surface potential barrier, a phenomenon called *field emission*. The field emission current is described by the Fowler–Nordheim equation (Fowler and Nordheim, 1928). Figure 5 shows the modified Paschen curve for air at 1 atm (Zhang et al., 2004a), in which the minimum and rise in breakdown voltage at small gap spacing is replaced with a plateau (the unmodified Paschen curve would have a minimum at ~5 μm gap spacing) and steep decline to zero. At the "knee" where the steep decline starts, field emission takes over completely from Townsend avalanche. The exact location of plateau and knee depends on the geometry, roughness, and composition of the metal electrodes. Finally, for ultrathin gaps smaller than ~2 nm, there is a finite probability that electrons can tunnel across an insulating barrier and result in a significant tunneling current.

Figure 5 indicates that breakdown in atmospheric pressure in very narrow gaps can occur at relatively low voltages, of a few tens of volts, which makes practical applications attractive. The situation becomes more favorable if one of the electrodes has a needle shape: The electrical field at the tip of the needle is intensified, and this leads to field emission at lower voltages than observed for the two planar electrodes of Figure 5. Work in our lab resulted in a factor 10 higher current density for a forest of

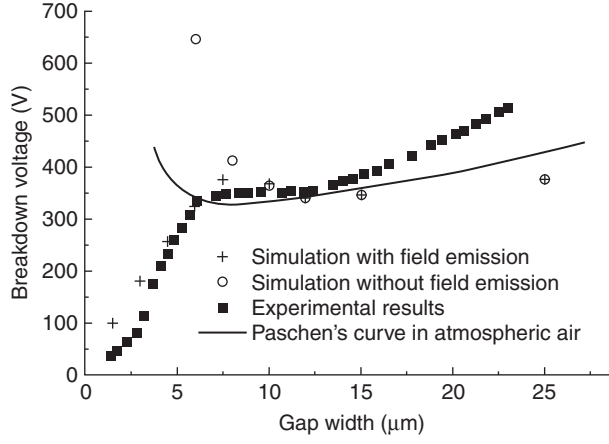

Figure 5 Paschen curve in atmospheric air, comparing simulation results with and without field emission, with experimental results (Zhang et al., 2004a; reproduced with permission).

tungsten oxide nanowires compared to a planar electrode at the same voltage (Ağiral et al., 2008a). Below we will show an example of the use of these nanowire electrodes in chemical synthesis. Another application of a combination of nanowires (carbon nanotubes (CNTs)) and a planar electrode is the recent work on miniaturized gas ionization sensors (Modi et al., 2003).

Figure 6 shows a typical field emitter design that consists of a sharp tip electrode and a *gate electrode*. This design is of the *Spindt type*, which refers to the fabrication process developed by Spindt et al. (1976). This design and others quite similar to it have become known for their application in plasma display devices, where the gate electrode acts as a counter electrode for the emitter electrode, and electrons emitted from the tip travel through a vacuum to hit a phosphorescent screen. The emission current at a given gate voltage strongly depends on the radius of curvature of the tip and the spacing between tip and gate, where the latter can be scaled quite easily by changing the gate hole opening. Reducing the size of this opening will give a higher emission current with a lower turn-on voltage. An example of this is a high-density array of field emitter tips (2.5×10^9 tips per cm^2) with an opening of 100 nm that can be driven by voltages of 10–20 V (Choi et al., 2001).

Field emitter tips with gate electrodes have not been applied for the generation of reactive species for chemical synthesis, and this may be an interesting field for future study, because of the extra flexibility that these devices may offer. Devices that go in this direction are the electron impact ionization sources used for mass spectrometers (Kornienko et al., 2000). A particularly interesting feature of gate emitters is the possibility of separating the region where electrons are generated (between the tip and the gate electrode) and the region where chemistry can be stimulated (just like in the plasma displays). One may think of focusing the electron beam on a catalyst surface to enhance surface reactions, or may use the space between tip and gate, if connected to an inlet hole which runs to the back of the glass base in Figure 6, to introduce a gas that will be

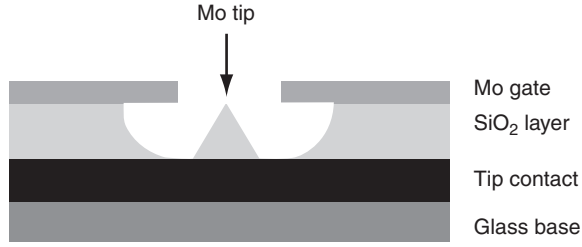

Figure 6 Field emitter tip of the Spindt type with an integrated gate electrode (Reuss et al., 2003; reproduced with permission).

ionized in or close to the gate opening. An exciting option would be a configuration in which each emitter-gate combination introduces a different gas. The high density of tips achievable may render the desired throughput of the system. Note also that if an array of individually addressable emitter tips is used, each emitter tip may be tuned to a different energy, allowing both a chemical gas-phase reaction to occur and ionization, if required at different locations and with a certain time interval.

2.2 Applications of microplasma reaction technology

Novel applications have been developed from the combination of microreactor technology and nonequilibrium microplasma chemistry. Here we discuss a selection from the recent literature on this topic to illustrate several main trends. We will focus on microplasmas in confined microchannels for the purpose of chemical synthesis and environmental applications.

2.2.1 Nanostructure synthesis in microplasma reactors

Synthesis of nanostructures using microplasma reactors is an attractive method since decomposition of the source material and subsequent crystal nucleation can be performed in the high-density nonequilibrium plasma within time intervals on the order of milliseconds. For example, Sankaran et al. (2005) synthesized silicon nanoparticles, 1–3 nm in diameter, from a mixture of argon/silane in a continuous flow atmospheric pressure microplasma reactor. Their technique is based on high pressure microdischarges with very short operation time (μs–ms). Microdischarges were created in a hollow cathode, which consists of a stainless-steel capillary tube with 180 μm ID (inner diameter) and extended toward an anode, a metal tube with 1 mm ID, as shown in Figure 7. Using a direct current microplasma which was sustained at 300–500 V and 3–10 mA, silicon nanoparticles were produced as an aerosol around atmospheric pressure. Since this microreactor operates at low powers (5–10 W) in plasma volumes less than 1 μl, resulting power densities were as high as 10 kW cm^{-3}. Such a high-density plasma allows fast plasma processing for the synthesis of blue luminescent silicon nanoparticles. The high density of energetic electrons in the microdischarges efficiently decomposed the gaseous precursor to produce radicals in the reaction zone. At a radical concentration high enough for nucleation, nanoparticles can start to grow in the microplasma. When the particles are removed by the gas flow from the discharge zone to a zone with a low concentration of radicals, particle growth will stop. An additional feature of the system is that particle charging in the microplasma reduces coagulation downstream of the reaction zone. Using the

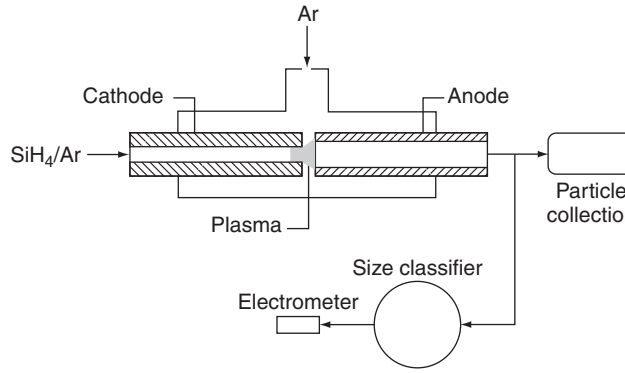

Figure 7 Schematic diagram of microplasma reactor for the synthesis of silicon nanoparticles. A microdischarge forms at the cathode tip and extends a short distance toward the anode (Sankaran et al., 2005; reproduced with permission).

same direct current microplasma technique, Fe and Ni catalyst particles were synthesized in a controlled way at atmospheric pressure and used for gas-phase growth of CNTs (Chiang and Sankaran, 2007, 2008). The catalyst particles were prepared from ferrocene and nickelocene. In summary, this simple and inexpensive microreaction technique can be used to synthesize nanoparticles in a continuous flow from the decomposition of gaseous precursors.

Nozaki et al. (2007a, 2007b) developed an atmospheric pressure microplasma reactor for the fabrication of tunable photoluminescent silicon nanocrystals (3–15 nm). They generated a capacitively coupled nonequilibrium plasma in a capillary glass tube with a volume of less than 1 µl and a residence time around 100 µs and used it to decompose silicon tetrachloride into atomic silicon. In the reactor a mixture of argon, hydrogen, and silicon tetrachloride was activated using a very-high-frequency (VHF, 144 MHz) power source. A schematic diagram of the experimental setup and an image of the microplasma reactor are shown in Figure 8. The upper electrode is connected to the VHF source (35 W discharge power) through a matching circuit and metallic electrodes with a 2 mm gap between them are around the outside of the capillary tube (borosilicate glass: ID = 630 µm, OD = 1,100 µm). Optical emission spectroscopic characterization of the microplasma indicated an electron density of 10^{15} cm^{-3}, an argon excitation temperature of 5,000 K, and a rotational temperature of 1,500 K. Under these high-density reactive conditions, efficient decomposition of the silicon source gas and formation of a supersaturated silicon vapor lead to nucleation of gas-phase crystals via three-body collisions and subsequent rapid termination of crystal growth due to the very short residence time in the microreactor.

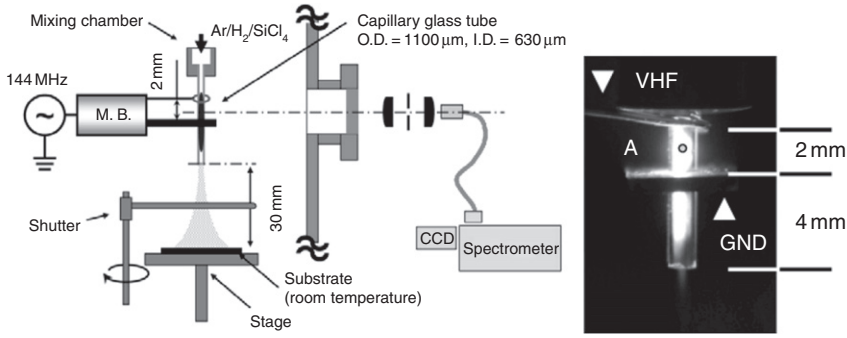

Figure 8 Schematic diagram of experimental setup and image of microplasma reactor with VHF source developed for the synthesis of photoluminescent silicon nanocrystals at room temperature (Nozaki et al., 2007a; reproduced with permission). M.B. is a matching electrical circuit.

An inductively coupled microplasma reactor was developed by applying ultrahigh frequency (UHF) to deposit a material on different substrates (Bose et al., 2006; Shimizu et al., 2003, 2005). An atmospheric pressure O_2–Ar microplasma reactor was used to prepare molybdenum oxide nanoparticles using molybdenum wire as the source material. The molybdenum metal wire with a diameter of 100 μm was inserted 6 mm from the exit of a pinched nozzle with an exit opening with an ID of 60–70 μm. A 20-turn copper coil was used to connect the reactor to the UHF source via a matching circuit. A drawing of the capillary microreactor is shown in Figure 9. A high-density

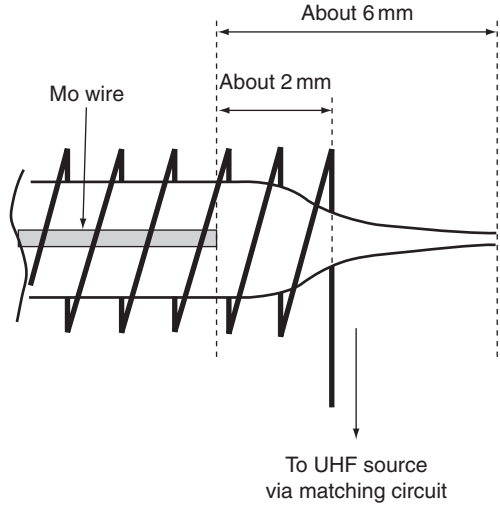

Figure 9 Capillary head of UHF microplasma reactor developed for the synthesis of molybdenum oxide nanoparticles (Bose et al., 2006; reproduced with permission).

microplasma oxidized the molybdenum and MoO_x nanoparticle seeds were supplied from the wire. The flow rate of the O_2–Ar mixture affected the process mechanism and therewith controlled shape, size, and oxidation state of the nanoparticles. It was found that MoO_2 oxidized to MoO_3 and that nanoparticle size decreased with an increase in flow rate. Using the same UHF microplasma technique, a tungsten wire was coated with multi-walled carbon nanotubes (MWCNTs) by flowing methane and vaporized ferrocene gases through a microchannel (Shimizu et al., 2005). This new microreaction method is unique as it gives a higher growth rate of MWCNTs with low power consumption (a few tens of watts) than conventional plasma-enhanced CVD processes.

Atmospheric pressure microplasma technology has the advantage of creating high-density reactive media in small spaces which can be used for surface modification and material deposition inside microchannels. We have recently developed a DBD technique to activate a coating of nickel/alumina catalyst in a capillary microreactor to enhance carbon nanofiber (CNF) growth on this coating (Ağiral et al., 2009). CNFs are promising nanostructured catalytic supports for liquid-phase reactions due to their high porosity and tortuosity (De Jong and Geus, 2000). Although thermal activation is an important way to significantly increase nanofiber yield, an atmospheric pressure microplasma may form an alternative route by using discharge-activated species which react at the catalyst surface at ambient temperatures. In our work, the fused silica capillary microreactor (500 μm ID, 550 μm OD) with an internal nickel/alumina catalyst coating was connected to a gas supply through a graphite ferrule high-voltage electrode. A DBD was generated to activate the catalyst at 300 K under a flow of hydrogen (5 ml min^{-1}) and helium (150 ml min^{-1}) for 15 min. The microreactor, catalyst coating, and microplasma treatment are shown in Figure 10. The catalyst color changed from light gray to dark gray after activation for 15 min showing that reduction of nickel took place during the discharge operation. Optical emission spectroscopic characterization showed that low-temperature activation of the catalyst occurs via active plasma species in the microreactor at atmospheric pressure. The discharge generated in the microchannel was characterized as uniform and stable with a high-power density (680 W cm^{-3}) at ambient gas temperature. The discharge treatment increased the CNF yield significantly compared to a nonactivated sample and the process can compete with a high-temperature treatment at 973 K for 2 h. Additionally, a comparison of the low-temperature microplasma treatment with a thermal treatment showed that the diameter of nanofibers is much more uniform in the former case. The method demonstrates the feasibility of cold catalyst activation on microreactor walls.

Another example of inner wall modification of microchannels with a microplasma is the deposition of uniform platinum films in microchannels

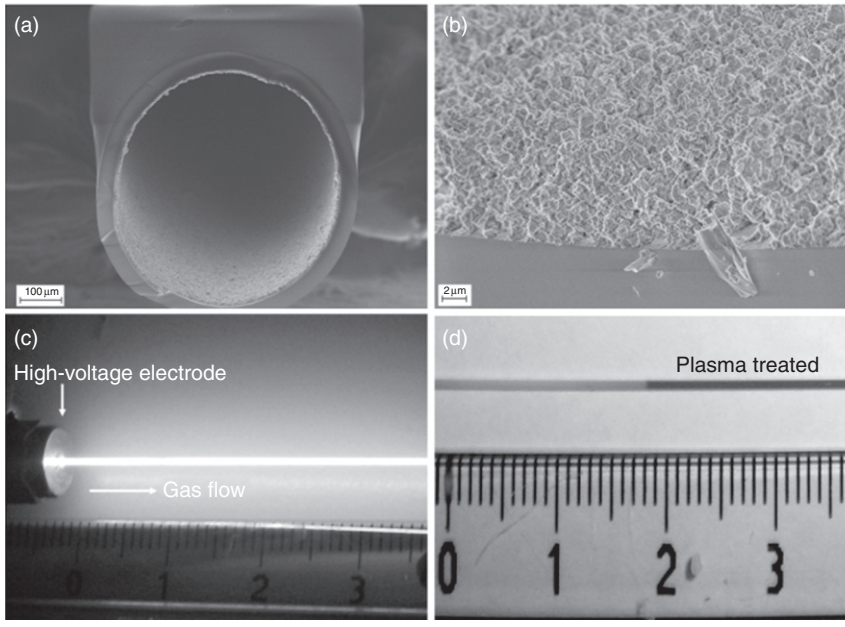

Figure 10 (a) SEM images of fused silica capillary microreactor coated with Ni/alumina catalyst, (b) catalyst layer after calcinations, (c) photo taken during microplasma treatment to increase catalyst activity for CNF synthesis, and (d) change in color of catalyst from light gray to dark gray after activation for 15 min (Ağıral et al., 2009; reproduced with permission).

(Kadowaki et al., 2006). This was done by generating a DBD at a low-pressure (a few Torr) in a capillary and in a microchannel in a glass chip, with electrodes attached to the outer surface along the channel axis. Photographs of the microplasma in the capillary and in the Pyrex chip are shown in Figure 11. Cylindrical graphite and metal foil electrodes were used for the capillary and the Pyrex chip, respectively. By introducing vaporized platinum bisacetylacetonate, plasma deposition led to a platinum film with a thickness of more than 100 nm. By controlling the voltage and frequency parameters, it was possible to achieve uniform deposition between the electrodes in the microchannel. This technique is a good example of the possibility of using microplasma technology to deposit a thin-film catalyst or other coatings in a controlled way in microreactors.

2.2.2 Environmental applications of microplasma reactors

Through the generation of highly reactive species such as energetic electrons and active radicals, microplasma reactors create novel process windows for C–C and C–H bond cleavage involved in the decomposition of harmful gaseous pollutants at atmospheric pressure. As an example of

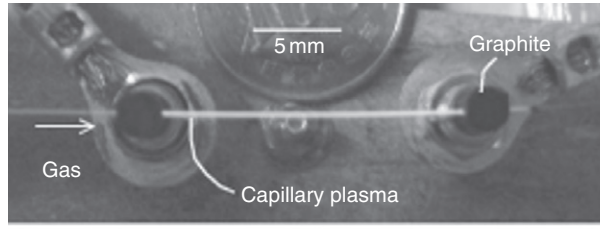

(a) Ar, 2 Torr

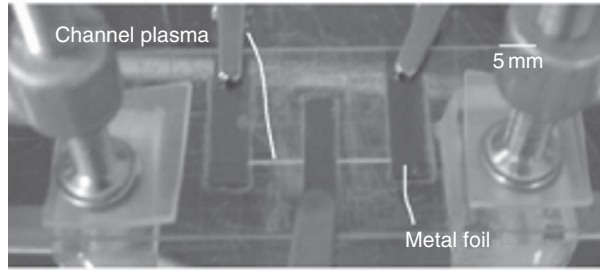

(b) He, 5 Torr

Figure 11 Photos of a microplasma in (a) a capillary and (b) a microchannel in a Pyrex chip, developed for plasma CVD of platinum films (Kadowaki et al., 2006; reproduced with permission).

this, a miniature DBD device was developed for the decomposition of volatile organic compounds (VOCs) (Seto et al., 2005). The device works with a surface discharge microplasma and contains microelectrodes manufactured by photoetching of stainless-steel foil and a dielectric substrate, acting as a barrier, made from a rectangular sheet of mica (Figure 12). By applying a high-voltage (3.5 kV) alternating current (AC) field (67 kHz) to the discharge electrode, a microplasma was formed on the surface of the mica sheet and high-energy electrons were generated which dissociated molecules, formed negative and positive ions, and excited molecular and

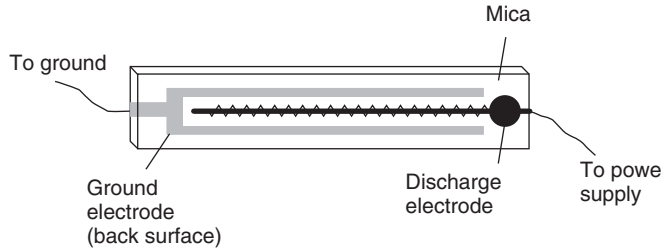

Figure 12 Illustration of a surface-discharge microplasma reactor developed for the decomposition of VOCs in the gas phase (Seto et al., 2005; reproduced with permission).

elemental species. Ion counting measurements showed that most of the by-products were negatively charged. The efficiency of toluene decomposition was found to be more than 99% in batch and 30–80% in continuous flow, and it was shown that toluene was completely converted into carbon dioxide by the atomic oxygen generated in the microplasma reactor.

Decomposition of tetrafluoromethane at atmospheric pressure was achieved with a microreactor which has very small electrode gaps (70 μm) between microstructured electrodes with an interdigitated arrangement (Figure 13) (Sichler et al., 2004). The merits of this reactor are low ignition voltages and a homogeneous plasma at high pressure. Alumina substrates, nickel electrodes, and Foturan® glass with an alumina coating were used as the microreactor materials. It was shown that micromachined flow structures provide effective flow control and have a large effect on decomposition efficiency. Additionally, scale-up to larger exhaust gas flows was achieved by "numbering up," that is, by constructing a multireactor with 16 microplasma reactors in parallel. Besides the larger throughput, the transition to a multireactor concept reduced the power strain on single microreactors and prolonged their lifetime. It was suggested that 25 of such multireactors are needed to treat 20 liter per minute of fluorinated waste gas for a small semiconductor plant, at an energy consumption of only 50% of that of a conventional combustion system.

Mori et al. used capillary discharge tubes with an ID of 0.5 or 3 mm to decompose carbon dioxide. The setup is shown in Figure 14 (Mori et al.,

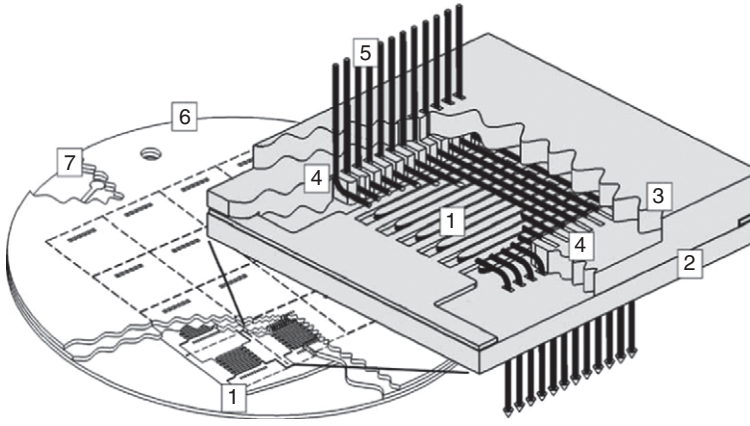

Figure 13 Illustration of a single microplasma reactor and its integration in a multireactor. Numbered features are (1) plasma source, (2) glass structure, (3) reaction chamber, (4) inlet and outlet of the reactor, (5) gas flow, (6) 4 × 4 array in a multireactor, and (7) contact pads for RF power (Sichler et al., 2004; reproduced with permission).

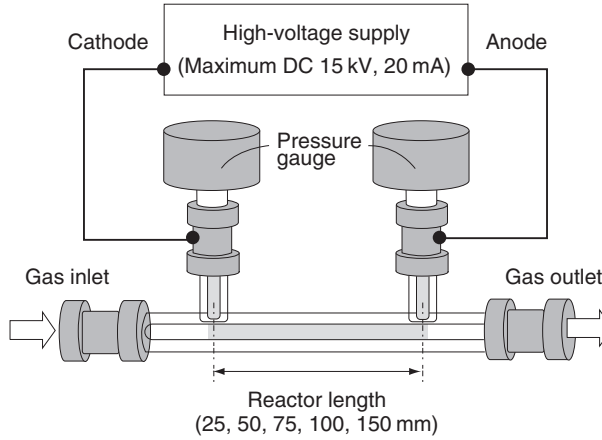

Figure 14 Schematic diagram of the capillary plasma reactor developed for the decomposition of carbon dioxide (Mori et al., 2006; reproduced with permission).

2006). The capillary plasma reactor consists of a Pyrex glass body and mounted electrodes which are not in direct contact with the gas flow in order to eliminate the influence of the cathode and anode region on CO_2 decomposition. Analysis of downscaling effects on the plasma chemistry and discharge characteristics showed that the carbon dioxide conversion rate is mainly determined by electron impact dissociation and gas-phase reverse reactions in the capillary microreactor. The extremely high CO_2 conversion rate was attributed to an increased current density rather than to surface reactions or an increased electric field.

The application of nanostructures as electrodes in a microplasma reactor was used to increase the reactivity and efficiency of barrier discharge processes at atmospheric pressure (Ağiral et al., 2008b). CNFs and tungsten oxide ($W_{18}O_{49}$) nanowires were integrated into a continuous flow microplasma reactor so that charge injection from the nanostructures by field emission supplied free electrons and ions after discharge. Incorporation of the nanostructures was performed by growing nanowires and nanofibers on the silicon chip which was used as a high-voltage electrode in a glass microreactor system, as shown in Figure 15. Atmospheric pressure field electron emission tests showed that field enhancement at the tip apex of the nanostructures results in electron emission in air. Injection of charged species during discharge generation results in a decrease in breakdown voltage and a higher power deposition, at the same measured potentials as applied on electrodes without nanostructures. As a model reaction, CO_2 cracking was tested and it was found that the chemical reactivity of the discharge is increased by application of the nanofibers.

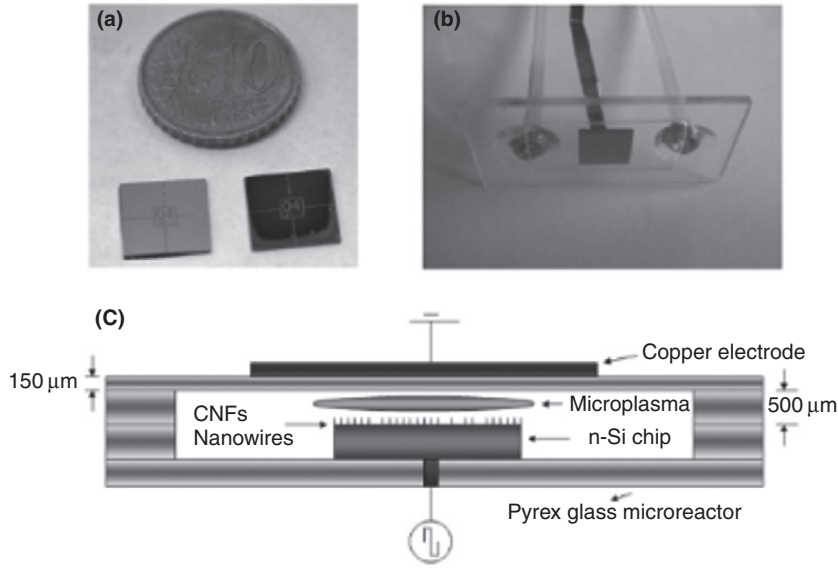

Figure 15 On-chip microplasma reactor using nanostructured electrodes, (a) silicon chip before and after a CVD process for nanostructure growth, (b) microplasma reactor, and (c) general diagram of the device (Ağıral et al., 2008b; reproduced with permission).

2.2.3 Chemical synthesis in microplasma reactors

Performing plasma processes in a continuous-flow microreactor leads to precise control of residence time and to extreme quenching conditions, therewith enabling control over the composition of the reaction mixture and product selectivity. In a nonequilibrium microplasma reactor, low-temperature activation of hydrocarbons and fuels, which is difficult to obtain in conventional thermochemical processes, can be achieved at ambient conditions.

Nozaki et al. (2004) described the application of a microplasma reactor in partial oxidation of methane. The plasma generation principle in this case is similar to a DBD and gives high-energy electrons which activate methane–oxygen mixtures for direct production of methanol. The microreactor consists of a Pyrex thin glass tube (ID = 1.0 mm, length = 60 mm) with a twisted metallic wire (ID = 0.2 mm, length = 100 mm) inside, as shown in Figure 16. Power consumption was calculated to be between 3 and 10 W. Excess heat generated by partial oxidation was efficiently removed from the microreactor, and successive destruction of formed oxygenates was minimized in the highly quenching environment. It was possible to produce methanol reproducibly in a one-pass process, with 10% maximum yield at room temperature, and at 100 kPa within 280 ms without explosion of the methane/oxygen mixture. The advantage of

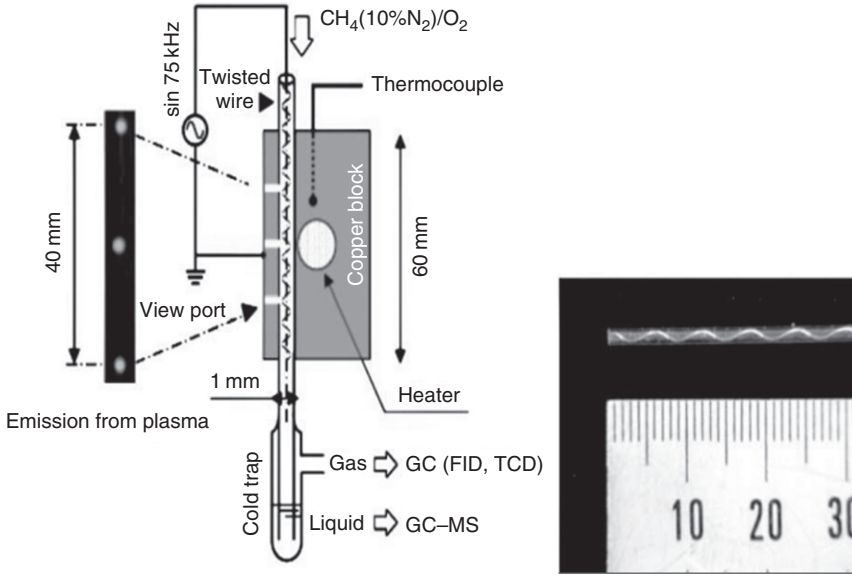

Figure 16 Microplasma reactor setup for partial oxidation of methane (left) and photo of thin glass tube equipped with a twisted metal wire (right) (Nozaki et al., 2007a; reproduced with permission).

using a plasma microreactor for fuel processing is that methane can be activated by high-energy electrons to achieve 40% conversion, independent of temperature and pressure. Additionally, unlike in thermochemical reactions, product selectivity is independent of methane conversion. However, the present microplasma reactor has not yet been made compatible with existing methanol manufacturing processes, and the reactor dimensions and power consumption need to be optimized in terms of a balance between excitation and quenching processes.

Hsu and Graves (2005) have used a micro hollow cathode as a microreactor to decompose ammonia and carbon dioxide. An MHCD can provide a highly reactive environment with a high electron temperature, power density, and ion density which would be ideal for endothermic cracking reactions. Decomposition of ammonia into nitrogen and hydrogen can be used as a source of pure hydrogen, while cracking of carbon dioxide can be used to dispose of radioactive carbon dioxide, or for the production of oxygen. In this case, the MHCD was constructed from two molybdenum electrodes (100 μm thick) sandwiching a mica dielectric (260 μm thick). The three layers were glued together and a 200 μm hole was drilled to construct a continuous flow microreactor. Significant decomposition of ammonia and carbon dioxide with effective reaction temperatures exceeding 2000 K was shown. As a demonstration of the numbering-up principle, it was shown that with two or more

microreactors in series the conversion could be increased significantly. This work demonstrated that microplasma-induced generation of hydrogen from ammonia in a flow-through MHCD is feasible, however, to become of economic relevance, the overall power efficiency should be increased. This may be done by pulsing the plasma, or operating many microplasma reactors in parallel and/or in series. It was proposed to pulse the discharge with short microsecond pulses to minimize electrical power input and stabilize the plasma.

Direct hydroxylation of benzene to phenol and of toluene to cresol in a microplasma reactor was carried out using a DBD at atmospheric pressure (Sekiguchi et al., 2005). This type of discharge provides hot electrons which dissociate molecules and therewith initiate hydroxylation reactions at ambient gas temperature. The glass microreactor studied by Sekiguchi et al. has a rectangular shape (100 mm in length and 70 mm in width) with aluminum electrodes and Teflon sheets as spacers, see Figure 17. Energetic electrons and oxygen radicals can dissociate the aromatic ring and functional groups, which is followed by oxidation. It was proposed that the selectivity and the yield of this plasma-based direct hydroxylation process

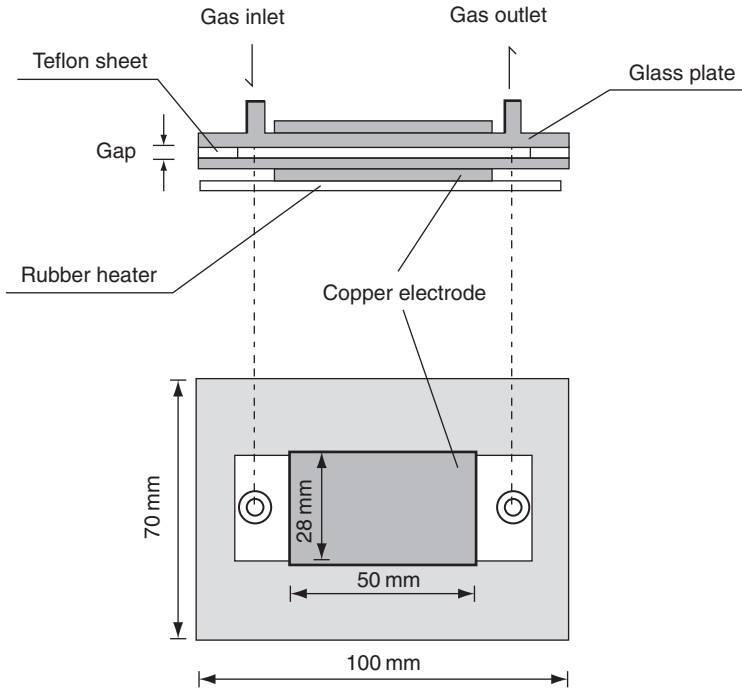

Figure 17 Schematic diagram of microplasma reactor, based on DBD, for hydroxylation of benzene and toluene (Sekiguchi et al., 2005; reproduced with permission).

may be increased by controlling the production of oxygen radicals via changes in the reactor surface or plasma generation methods.

Oxidative conversion of light alkanes, C_1–C_3 range, was carried out in a dielectric barrier-type microplasma reactor (Trionfetti et al., 2008a). The direct conversion of alkanes is largely obstructed by the strong C–H (415 kJ mol^{-1}, for methane) and C–C bonds (350 kJ mol^{-1} for ethane) (Choudhary et al., 2003). Cold plasma processing can be an alternative to high-temperature thermochemical processes. A barrier discharge treatment in a confined reactor offers the advantages of a uniform and dense plasma with a better control of residence time. The tested microplasma reactor (30 mm length, 5 mm width, and 500 μm channel depth) was fabricated by thermal bonding of three Pyrex layers and attaching copper electrodes on top and bottom at the outside of the chip, as shown in Figure 18. A plasma was generated by applying a high-voltage (5–10 kV) sine wave (60 kHz) to the top electrode while the bottom electrode was grounded. Heat produced during the oxidative conversion of alkanes was easily removed due to the small volume and high surface area of the microreactor, so that it operated at ambient temperature. The feed composition was 10% alkane and 1% oxygen in helium. Activation of hydrocarbons follows two main routes. In the first one, energized electrons dissociate alkane molecules by cleaving C–H and C–C bonds. The direct observation of CH, C_2, and H excited species by an optical emission spectrometer is an indication of this bond cleavage at room temperature. Secondly, electron impact dissociation of oxygen molecules produces active oxygen radicals which initiate radical chain reactions. Excited helium species also may play a role in the process, by transferring energy to alkane and oxygen molecules. In the experiments with propane, a high selectivity (37%) to products with a molecular weight higher than propane (C_4, C_4^+) was observed, indicating that under microplasma conditions C–C bond formation occurs. Coupling reactions between radicals are favored at lower temperatures and the cold plasma process in a

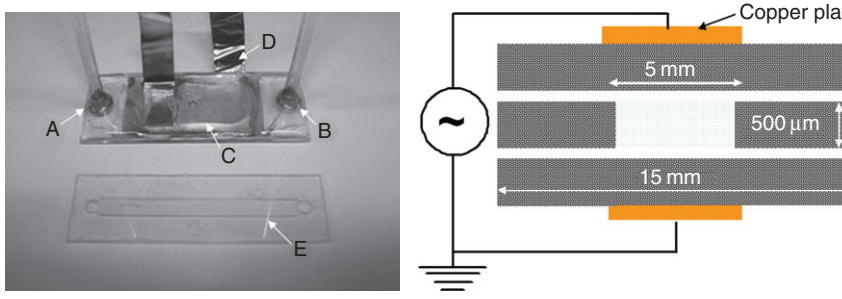

Figure 18 Microplasma reactor, based on DBD, for oxidative conversion of C_1–C_3 alkanes; A: gas inlet; B: gas outlet; C: frontside copper electrode; D: backside electrode (Trionfetti et al., 2008a; reproduced with permission).

microreactor could be an alternative for upgrading light hydrocarbons by direct homologation of alkanes. A kinetic model of plasma propane conversion in this microplasma reactor was developed for better understanding of physical and chemical processes over a range of reactor operation conditions (Ağıral et al., 2008c). The model employed the well-mixed plasma reactor module of Chemkin 4.1 (CHEMKIN, 2004) to determine the time-averaged species composition and electron energy balance which equates the rate of change of the electron swarm internal energy to the net flow of electron enthalpy into and out of the reactor, therewith accounting for net chemical production rates, surface losses, collisional losses, and power deposition from the externally applied electromagnetic field. Reaction rate coefficients of electron impact reactions with propane were determined with the aid of BOLSIG+ software (Hagelaar and Pitchford, 2005). This software also calculates the relation between the average electron energy and the reduced electric field inside the microreactor. The estimated average electron temperature was used to obtain a steady-state solution in the Chemkin plasma reactor model. The BOLSIG+ code uses the two-term spherical harmonic expansion of the electron energy distribution function to solve a zero-dimensional Boltzmann equation. Cross sections of partial dissociative excitation and ionization processes ($e^- + C_xH_y$, $x = 1–3$; $y = 1–8$) were obtained from the experimental data of total dissociation cross sections and of total cross sections for dissociative ionization (Janev and Reiter, 2004). It is necessary to correct the residence time since a barrier discharge consists of filaments, and this was done on the basis of a quantitative agreement with experimental data. The model includes electron impact dissociation and ionization, ion–neutral reactions, neutral–neutral chemistry, and surface recombination of ions at the walls. Simulated results were compared with experimental data and a good agreement was found. H, CH, CH_2, CH_3, C_2H_3, C_2H_5, C_3H_5, C_3H_7, and C_4H_9 radicals were found to play an important role during propane conversion in the microplasma reactor. At higher propane conversion levels, enhanced C–C bond formation was observed.

The same microplasma reactor was used to study the feasibility of oxidative dehydrogenation of propane in the presence of a Li/MgO catalyst (Trionfetti et al., 2008b). It was anticipated that a synergistic effect between catalytic and plasma processes may be obtained, that possibly may give a higher conversion and yield of target products. The reason for this expectation was based on the following: First of all, a catalyst supported on an insulator oxide deposited in the barrier discharge region may influence the plasma properties due to a change in surface properties and permittivity of the dielectric material, and this influence may be positive. A well-chosen catalyst will, as always, decrease the overall activation energy, but the selectivity of a catalytic reaction may be increased by selective plasma activation of specific molecular bonds between

adsorbed species and surface. This can be thought to occur as follows: In a nonequilibrium plasma, molecules are excited by electron impact. Among the characteristic species (electrons, ions, molecular fragments and excites species such as electronic, vibrational, rotational/translational excitations), only radicals and vibrationally excited species will be relevant for surface reactions in an atmospheric pressure nonequilibrium plasmas, due to the fact that radicals have long relaxation times compared to the time needed for chemical reactions, plus that they have a high sticking probability on surfaces. Vibrational activation in the dissociation degree of freedom can lower the activation barrier for dissociative adsorption (Tas, 1995).

In addition to the above, in a microplasma reactor a more intensive interaction of plasma and catalyst surface can be achieved in a confined environment. Li/MgO catalysts in the presence of oxygen at high temperatures have [Li^+O^-] defect sites which activate C–H bonds in alkanes (Wang and Lunsford, 1986). Propane activation starts with hydrogen abstraction by oxygen ions, forming propyl radicals (Balint and Aika, 1997), C–C and C–H bond cleavage happens at high temperatures ($T > 823$ K) in the presence of [Li^+O^-] centers. At these temperatures, a loss of catalyst area was observed, which results in less heterogeneous formation of propene (Trionfetti et al., 2006). A microplasma reactor may allow initial propane activation at lower temperatures by enhanced radical surface interactions in the confinement of a microreactor. To test this, a Li/MgO catalyst was deposited on the surface of a glass microchannel by micropipetting a sol–gel precursor system. The catalytic microplasma reactor showed enhanced olefin selectivity in the presence of Li/MgO, which indicates the formation of defect sites at ambient temperatures. Formation of higher hydrocarbon products ($C_4 + C_4^+$) showed that coupling of radicals occurs predominantly in the homogeneous phase.

Anderson et al. (2008) have fabricated plastic microreactors based on parallel linear arrays of interconnected cylindrical microcavity plasma devices, using replica molding in UV-curable polymers. Their study was aimed at on-chip plasma processing with the generation of gas or solid phase from a gas feedstock. Figure 19 shows a magnified view of the 10×10 arrays of 400 μm diameter microplasma devices, operating in 600 Torr of Ar. Deposition of $(C–S)_n$ microstructured polymer was done in Ar/CS_2 plasma. This study showed the feasibility of using low cost and disposable polymer microplasma reactors for potential chemical synthesis applications.

2.2.4 Generation of plasma in a liquid or at a liquid interface

Although, as was discussed above, plasma and other discharges are usually discussed in the context of gas-phase processes, electrical discharges are also quite well studied in *liquids*. For example, liquid-phase discharge reactors have recently been applied in drinking water and

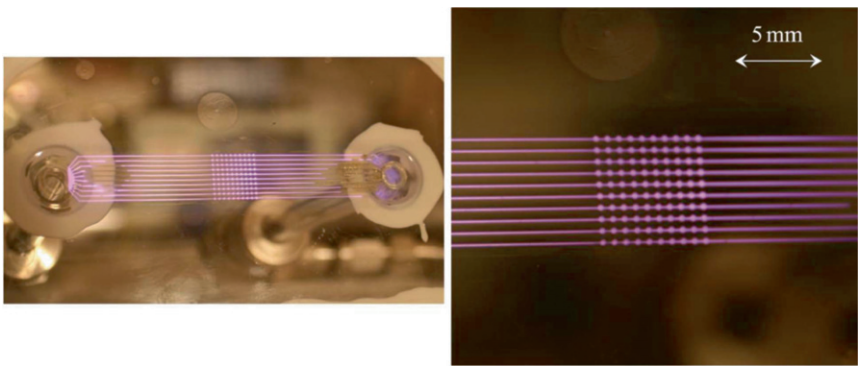

Figure 19 Photographs of microplasma reactor fabricated by replica molding on a plastic substrate (left) and magnified view of the 10 × 10 array of 400 μm diameter microcavity plasma channels, operating in argon (right) (Anderson et al., 2008; reproduced with permission).

wastewater treatment (Locke et al., 2006). Electric fields applied to water, called *electrohydraulic discharge*, initiate both chemical and physical processes, with two basic discharge types, differing by the amount of energy deposited in the system. The *corona* system uses discharges of ~1 J per pulse and operates at high frequency, 100–1000 Hz, with a peak current below 100 A and nanosecond voltage rise times. The *pulsed arc* discharge uses energy of ~1 kJ per pulse and larger, and operates at low frequency, 10^{-2}–10^{-3} Hz, with a peak current above 1 kA and microsecond voltage rise. The pulsed arc generates strong shock waves accompanied with cavitation and bubbles with ionized gas inside, leading to chemical reactions that have been suggested to be similar to those that occur in sonochemistry. In the corona discharge a streamer is generated, relatively weak shock waves are formed and a moderate amount of bubbles is observed. Radicals and reactive species are formed in the narrow region near the corona discharge electrodes: Generation of H, O, and OH radicals were observed by emission optical spectroscopy (Locke et al., 2006).

Corona discharges in liquids can be generated in many different reactor configurations (Locke et al., 2006), but principally they fall into two categories (Figure 20), one in which both electrodes are immersed in the liquid, and one in which one of the electrodes is above the liquid. For the second configuration, ions, radicals, and neutral species produced by the discharge, which partially occurs in the gas phase, may transfer into the liquid phase through action of the electric field, and react there to form other reactive species. It was suggested that the average energy of the positive gaseous ions entering the liquid phase may be more than 100 eV.

Note that the configurations in Figure 20 involve *point electrodes*. To initiate a pulsed discharge in water, it is necessary to have a high-intensity electric field (10^7–10^9 V m^{-1}) at the tip of the electrode. Proper insulation of the electrode is essential, because water is much more conductive than air. A small protrusion of the point electrode from the insulator surface

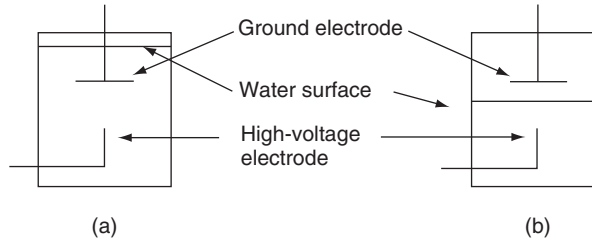

Figure 20 Schematic of two configurations for a pulsed corona reactor: (a) ground electrode submerged in liquid and (b) ground electrode suspended above the liquid surface. The immersed electrode in both cases is a point electrode (reprinted with permission from Grymonpré et al., 2004; Copyright 2004 American Chemical Society). For a variety of other reactor configurations, see Locke et al. (2006).

(less than 1 mm) gives a better discharge, because the electric field concentrates near the electrode edge or interface between the metal and the insulator. In air or gas insulation is less important, because the air surrounding the needle is a very good insulator.

As an example of an application of a gas–liquid pulsed corona discharge reactor, Grymonpré et al. utilized high-voltage needlepoint electrodes submerged in water coupled with a planar ground electrode in the gas phase above the water to remove low concentrations of phenol (Grymonpré et al., 2004). They found that the liquid-phase discharge leads to the formation of hydrogen peroxide and hydroxyl radicals, and the gas-phase discharge leads to the formation of ozone. A reticulated carbon electrode produced a higher number and more uniform distribution of streamers in the gas phase, which gave a higher amount of ozone dissolved in the liquid phase.

Other examples of gas–liquid electrical discharges are the degradation of 4-chlorophenol in water with bubbling air, in a multipoint-plate pulsed high-voltage reactor (Lei et al., 2007), and flue gas desulfurization by corona discharge in a cylindrical reactor with a wetted lining (Jiang et al., 2006) (*note that this is a typical microreactor configuration*). Corona discharge with a wet interface, but in a different reactor design, has been developed for industrial-scale desulfurization (Yan et al., 2006). The concept is based on a partitioned wet reactor system in which SO_2 in the flue gas is absorbed with ammonia water in a repeated spraying process, and then transferred at an appropriate flow rate to the successive plasma reaction stage in which uniformly distributed streamers are generated, in which the sulfites in the solution undergo plasma oxidization. The resulting output liquid is dried to produce a powder product using heat produced in the reactor. An interesting claim by the authors (unfortunately only mentioned in the abstract of the paper and not elaborated further) is that SO_2 absorption by the liquid is enhanced by *electric wind*, a concept to be discussed in a following section.

Just as was the case for gas-phase plasma devices, miniaturization of gas–liquid discharge reactors has several advantages, the most important being the possibility to keep the voltages for initiation of streamers or other discharge characteristics low, and the possibility to work at high pressures (atmospheric or higher) instead of vacuum. As was discussed above, the best results for larger systems have been obtained for needle electrodes, which one may also consider a step toward miniaturization.

One particular example of what may be called a gas–liquid discharge microreactor is the work of Baba et al. (2006, 2007), who have demonstrated the generation of an atmospheric pressure glow-discharge plasma in contact with liquid paraffin, using a capacitively coupled plasma method. The choice for paraffin has two reasons: no hydroxyl group present (which is thought to capture electrons, as is the case in water)

and low volatility. Two types of plasma source, a mesh electrode-type and a parallel wire electrode-type, were applied, with typical electrode distance of 500 μm for the mesh and 1–5 mm for the parallel wire. The configuration was of the type (b) in Figure 20, with the mesh or parallel wires immersed in the liquid. Optical emission measurements showed evidence of CH and C_2, originating from paraffin, while laser-Raman scattering spectroscopy revealed that a graphitic soot-like material is produced.

Another microfluidic example in which a plasma is generated at a liquid–gas interface, is the work on a miniaturized discharge device for atomic emission, called electrolyte as a cathode discharge . This concept was developed to solve the problem of achieving adequate sample transport from the liquid to the gas phase, for analysis in a plasma detector comparable to the earlier analytical gas-phase microplasma devices (Eijkel et al., 1999). Conventional emission spectroscopy techniques achieve liquid sample introduction by nebulization of some sort or by drying the sample on one of the discharge electrodes, but such methods are not easily applicable in miniaturized analytical plasma devices. The desire remains to analyze a continuous liquid stream from a microchannel, as it would allow low-dead-volume in-line analysis of fractions from, for example, a microfluidic separation column. Figure 21 shows a schematic drawing of the developed device (Jenkins et al., 2005). Although this was meant to be used only for analysis, one can easily imagine using such a device (in a parallel format, to generate throughput) for the purpose of chemical synthesis.

Probably because the field is relatively young, not much has been reported yet on gas–liquid discharges in a microfluidic (microreactor) format. Yamatake et al. have used a DC-driven atmospheric plasma micro hollow cathode to directly inject O radicals into a fast oxygen gas

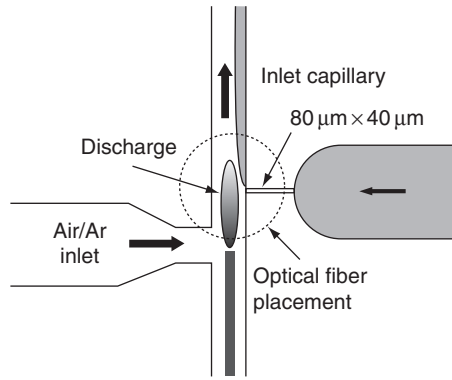

Figure 21 Schematic of aqueous electrode chip design (Jenkins et al., 2005; reproduced by permission of the Royal Society of Chemistry).

stream which was introduced in a solution of acetic acid, as a model for water treatment. A clear correlation was found between acetic acid decomposition rate and gas-flow velocity, which indicates that rapid injection of the key radical, which is thought to be O and which has a short lifetime in atmospheric oxygen, at the gas–liquid interface is crucial (Yamatake et al., 2006).

A interesting option would be the use of segmented flow (Taylor flow) patterns in a microchannel (Günther et al., 2004) in combination with a DBD as described above. Effectively, such a configuration may lead to similar chemistry as in a sonochemical process, but probably with a much higher efficiency, since the gas holdup volume in a microchannel with Taylor flow can be made much higher. An example of a discharge accomplished over a bubble train, but based on a conventional bubble column (see Figure 22) has recently been reported (Katayama et al., 2009).

A final topic to be discussed in this section is the direct injection of electrons into a liquid by the use of *nanowires*. The difference with the discharge processes described above for the point electrodes is twofold: the use of *nanostructured electrodes* and the generation of *solvated electrons*, instead of the initiation of a discharge. Solvated electrons have a very short

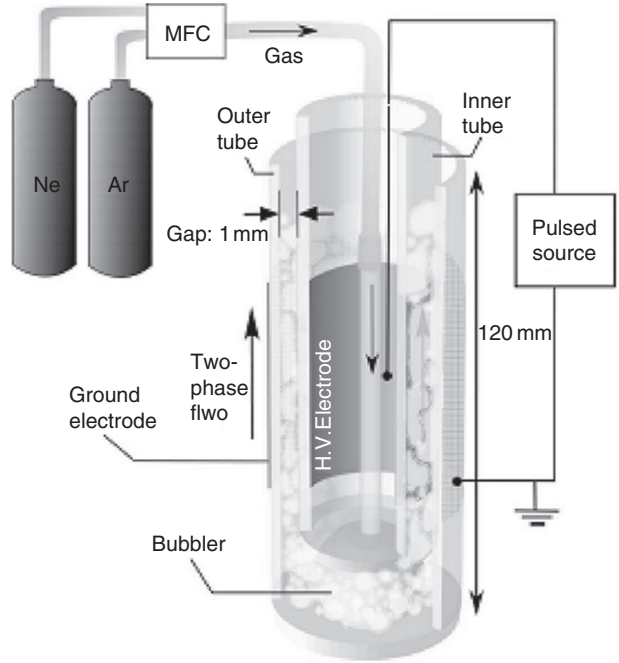

Figure 22 Schematic diagram of a DBD reactor, in which a discharge is carried out over a bubble column (from Katayama et al., 2009; © 2009 IEEE).

lifetime in water, on the order of 50 fs, due to the fast response of the hydrogen bond network (Bragg et al., 2004), but they may be stable for hours to months in other liquids, like liquid NH_3 (Jortner and Kestner, 1973).

In very pure nonpolar dielectric liquids, electron injection currents at very sharp tips follow the Fowler–Nordheim voltage dependence (Halpern and Gomer, 1969), just as is the case in solid insulators, and in a gas, as described before. In a study of the electrochemical behavior of CNT cathodes (Krivenko et al., 2007) direct experimental proof was found of electron emission into the liquid hexamethylphosphortriamide, which was chosen because it is a convenient solvent for the visualization of solvated electrons at room temperature: the solution will show an intense blue coloration upon the presence of solvated electrons. Electron spin resonance showed prove of a free electron. Electrogenerated (as opposed to photogenerated) solvated electrons have been used in the synthesis of L-histidinol (Beltrá et al., 2005), albeit that in that work the electrons were generated electrochemically from a solution of LiCl in $EtNH_2$, which is a solvent that is easier to handle than liquid ammonia (boiling points at atmospheric pressure are 17 °C and –33.34 °C, respectively).

These results suggest that the use of nanofiber electrodes in a microreactor environment to generate solvated electrons for chemical synthesis, may offer an interesting new route for reduction reactions. We are currently working on this concept in our laboratory (Ağiral et al., 2010).

3. ELECTROCHEMICAL MICROREACTORS

Electrochemistry, to distinguish it from the topics discussed in previous sections, is concerned with *low-energy charge transfer in solution*. The electron transfer typically occurs on the surface of a charged (usually metal) electrode. Possible chemical reactions that may occur, and that may be of importance in chemical synthesis, are the generation or annihilation of gases (in an electrolysis or a fuel cell, respectively) and the generation or neutralization of ions, which may be accompanied with the dissolution or deposition of a solid material.

The reasons to perform electrochemistry, in particular, *electrosynthesis*, in a *microfluidic system* are the following (Rode et al., 2009): (1) reduction of ohmic resistance in the electrochemical cell, by decreasing the distance between anode and cathode, (2) enhancement of mass transport by increase of electrode surface to cell volume ratio, also realized by small interelectrode gaps, (3) performing flow chemistry to establish single-pass conversion, and (4) coupling of cathode and anode processes, permitting simultaneous formation of products at both electrodes. The latter

possibility is very interesting from a sustainability point of view (less waste) and examples have started to appear in recent literature, like the epoxidation of propylene (Belmont and Girault, 1995). Paddon et al. have recently reviewed paired and coupled electrode reactions for electroorganic synthesis in microreactors (Paddon et al., 2006).

A fifth reason for using microfluidics in electrochemistry would be the possibility to combine flow chemistry with an ultrafast mixer, which allows the generation and subsequent use of short-lived reactive ions or radicals, for example, in a "cation flow" process (Suga et al., 2001; Yoshida, 2008). Finally, a sixth reason for performing electrochemistry in a microfluidic system may be the desire to efficiently remove reaction heat (or joule heat due to high currents in combination with a high ohmic resistance) in fast electrochemical reactions (Yoshida, 2008).

The research on electrochemistry in microreactors has been reviewed in a number of recent publications (Hessel et al., 2004; Rode et al., 2009; Yoshida, 2008; Yoshida et al., 2008); therefore, we do not want to go into too much detail here. But since these reviews almost exclusively concern electroorganic synthesis, a number of other applications will be highlighted here.

A specific type of electrochemical microsystem, although not directly a synthetic microreactor, is a *microfluidic fuel cell*. In a recent review (Kjeang et al., 2009), the developments and challenges in this field have been analyzed. Kjeang et al. define a microfluidic fuel cell as a fuel cell with fluid delivery and removal, reaction sites, and electrode structures all confined to a microfluidic channel. Most microfluidic fuel cells use colaminar flow, without a physical separation (like a membrane) between anode and cathode. The laminar flow characteristic is utilized to delay mixing of fuel (the anolyte) and oxidant (the catholyte), which occurs by diffusion only and is restricted to a small zone close to the anolyte–catholyte interface at the center of the channel. Electrodes are positioned on the walls of the channel, at sufficient distance from the diffusion zone in order to prevent fuel crossover. Both anolyte and catholyte contain supporting electrolyte which facilitates ionic transport. Figure 23 shows a specific example of a microfluidic fuel cell, namely one in which an air breathing cathode is used to eliminate one of the main problems with microfluidic fuel cells, that is, the mass transport limitation at the cathode in cases where dissolved oxygen is used as the oxidant.

The colaminar configuration has a number of advantages over other fuel cell designs: (1) mixed media operation, (2) operation at room temperature, and (3) no auxiliary humidification, water management, or cooling systems. Additional advantages may arise from the specific possibilities that micromachining offers, for example, special electrode designs like tapered electrodes to accommodate the downstream growth of the mixing zone and maximize fuel utilization (Bazylak et al., 2005) or

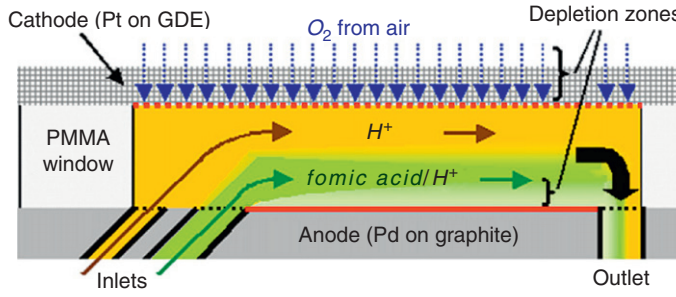

Figure 23 Air-breathing microfluidic fuel cells showing the colaminar flow principle, in combination with oxygen capture via gas diffusion through a porous cathode A three-phase interface is established between gas, electrolyte, and catalyst/solid electrode (reprinted with permission from Jayashree et al., 2005. Copyright 2005 American Chemical Society).

inlet and outlet manifolds for active control of concentration boundary layers by removing consumed species or adding reactants, respectively (Yoon et al., 2006). Despite all these advantages, current microfluidic fuel cells still have a too low-energy density (i.e., energy output per system volume or mass) to be of real practical value, which is mainly due to the single-pass use of electrolyte. An important issue in flow electrochemistry is the elimination of the supporting electrolyte that is added to enhance ionic transport. This electrolyte causes separation problems and product contamination. One option to minimize supporting electrolyte is to use a two-phase flow microfluidic system in which the reagent flow and the supporting electrolyte flow are kept separate. An example is the use of a two-phase flow with *N*-octyl-2-pyrrolidone (NOP) and aqueous electrolyte and with acetonitrile and aqueous electrolyte, in contact with a polycrystalline boron-doped diamond electrode (MacDonald et al., 2009). Two different configurations are possible: The first applies *pre-electrolysis*, in which the aqueous phase is oxidized to form ozone, bromine, peroxocarbonate, or the-like, before contact with the organic reactant phase, while the second has an aqueous and an organic phase, which contains the electrochemically active reagent, simultaneously in contact with the working electrode. Only a thin reaction zone close to the *triple-phase boundary zone* is active during the electrochemical reaction. The high electrical resistance within the organic phase restricts the reaction zone. Both configurations give clean electrosynthesis without electrolyte included in the organic phase, but the acetonitrile system gave better results due to its lower viscosity, which enhances mass transport and conversion rate, and its more stable triple-phase boundary electrolysis zone, with virtually no *undercutting* of the organic phase under the aqueous phase like it has been observed for NOP. Undercutting is a result of surface tension changes during electrochemistry (MacDonald et al., 2007). Electrochemistry at static triple-phase boundaries was also

demonstrated using droplets (Banks et al., 2003; Marken et al., 1997; Scholz et al., 2005), porous host electrodes (to optimize triple-phase boundary zones) (Ghanem and Marken, 2005; Niedziolka et al., 2007), microwire-based electrodes (Bak et al., 2007), and microdroplet arrays on lithographically modified electrode surfaces (Rayner et al., 2007).

A similar distinction between a system with pre-electrolysis with only one electrode (in this case anodic) process, and a system with simultaneous anodic and cathodic processes (in which anode and cathode are on opposite walls of a microchannel so that each liquid is only in contact with the desired electrode potential, analogous to the fuel cell configurations discussed above) was made by Horii et al. (2008) in their work on the *in situ* generation of carbocations for nucleophilic reactions. The carbocation is formed at the anode, and the reaction with the nucleophile is either downstream (in the pre-electrolysis case) or after diffusion across the liquid–liquid interface (in the case with both electrodes present at opposite walls). The concept was used for the anodic substitution of cyclic carbamates with allyltrimethylsilane, with moderate to good conversion yields without the need for low-temperature conditions. The advantages of the approach as claimed by the authors are efficient nucleophilic reactions in a single-pass operation, selective oxidation of substrates without oxidation of nucleophile, stabilization of cationic intermediates at ambient temperatures, by the use of ionic liquids as reaction media, and effective trapping of unstable cationic intermediates with a nucleophile.

An interesting development is the coupling of an electrochemical microreactor with a continuous separation process. Performing a synthetic chemical process in a continuous flow microreactor is now well established, but in the end the benefits of continuous processing will be lost if not also the downstream work-up processes can be performed in a continuous fashion. That is why at the moment a large research effort is devoted to coupling (or integrating) separation methods with microreactors (see Hartman and Jensen, 2009 for a recent review). An example is the coupling of a microreactor for electroorganic synthesis, configured as an electrochemical thin layer cell, to a *simulated moving bed* (SMB) separator (Küpper et al., 2003; Michel et al., 2003). SMB technology is a preparative chromatographic method which is turned into a continuous process by simulating a counterflow of the adsorbing stationary phase (a particle bed) and the mobile phase, by leaving the adsorbing phase unmoved but switch the positions for inlet of eluent and feed, and for outlet of raffinate and extract (Ruthven and Ching, 1989). In the work of Küpper et al., the SMB process has not been implemented, but the electrochemical reactor is designed to be operating with a conventional SMB plant (Küpper et al., 2003). Michel et al. describe a combination of electrochemical reaction and chromatographic SMB separation applied to the direct electrochemical production of arabinose and simulate its operation. The electrochemical

microreactors are placed between the chromatographic columns. The concept has the advantage of being able to switch the electrochemical reactors on and off by means of the applied current. Also in this work no experimental verification of the concept is given, but the models prove the feasibility of the integrated process, as higher yields than with a serial connection of reactor and SMB can be obtained, although the integrated process will obtain high productivity only at low yield and vice versa.

Micro-SMB separators have only been studied numerically (Subramani and Kurup, 2006), but one can think of ways to implement a *real* moving bed in a miniaturized version by applying a shifting magnetic field on, for example, magnetic resin beads or applying DEP on adsorbent particles, in a microchannel.

As a final topic for this section on electrochemical microreactors the electrochemical generation of cofactors in biocatalytic microreactors is worth mentioning. The use of immobilized enzymes has progressed rapidly in medical and analytical applications and in the food and beverages industry biocatalysts are used in a variety of processes and products. Immobilization of enzymes has the advantage over dissolved enzymes of easy recovery and reuse and (in many cases) improved stability. It is therefore not surprising that microreactors applying immobilized enzymes as a biocatalyst have received increasing attention in the recent literature.

For optimal operation enzymes may need the assistance of cofactors, for example, many of the dehydrogenases require nicotinamide adenine dinucleotide ($NAD(P)^+/NAD(P)H$). Because of the considerable cost of this cofactor, continuous regeneration is desired, which is possible by electrochemical regeneration from NAD^+ using a mediator (e.g., flavin adenine dinucleotide, FAD) which transports electrons from a cathode to an enzyme (e.g., formate dehydrogenase, FDH) which in its turn regenerates NADH from NAD^+. $FADH_2$ rather than formate serves as the substrate for the enzyme FDH, and enough $FADH_2$ can be generated at the electrode in order to shift the unfavorable equilibrium to NADH formation. However, due to the reverse reaction, which runs spontaneously at pH 7, the concentration of electrochemically generated $FADH_2$ remains low in the bulk solution in classical batch reactors, which is why *in situ* and local generation of $FADH_2$ is preferably performed in a microfluidic reactor (Yoon et al., 2005). The microreactor reported by Yoon et al. utilizes multistream laminar flow to focus a reagent-containing stream close to an electrode, by adjusting the flow rate ratio of reagent and buffer stream flowing in parallel. $FADH_2$ is indeed produced in sufficiently high concentrations at the electrode to drive the subsequent reaction toward NADH regeneration. Another example of the same mediator concept is the regeneration of NADH in a filter-press microreactor with electro-eroded cylindrical microchannels (Kane and Tzédakis, 2008). The high specific surface area of the cathode of $250\,cm^{-1}$ in this microreactor provided the desired conditions to increase

the $FADH_2/FAD$ concentration ratio and shift the nonspontaneous reaction $FADH_2/NAD^+$ toward regeneration of NADH. Both reactors (Kane and Tzédakis, 2008; Yoon et al., 2005) were tested for the synthesis of chiral L-lactate from pyruvate in the presence of L-lactate dehydrogenase.

A completely different example of cofactor generation in a microsystem is the local production of magnesium ions to control the position of activation of a DNA restriction enzyme (Katsura et al., 2004). Alternative DNA restriction schemes are important to cut DNA at specific positions, different from the conventional molecular biological methods. Control of restriction was achieved by applying a direct current to a needle electrode of magnesium. Only when and where the magnesium ions from this needle were produced, the restriction enzyme became activated.

4. ELECTROKINETIC CONTROL OF CHEMICAL REACTIONS

Instead of directly using the charged or otherwise electrically activated species in a chemical reaction, the option exists to use charges to *enhance mass transport*. This can be achieved by transporting the chemical species, if charged, themselves, or by transporting the medium in which the chemical species are contained. This *electrokinetic transport* exists in different forms, which will be highlighted below.

4.1 Electrophoresis and electroosmosis

In case an electric field is applied on an electrolyte in, for example, a glass tube, two different responses to the electric field will occur:

1. *Electrophoresis*: the positive ions in the electrolyte will move in the direction of the electric field E, while the negative ions will move in the opposite direction. The velocity v_{EF} by which the ions move is proportional to their electrophoretic mobility, μ_{EF}:

$$v_{EF} = \mu_{EF} E \tag{1}$$

   Electrophoretic mobilities are typically in the range of $3\text{–}8 \times 10^{-4}\,cm^2\,V^{-1}\,s^{-1}$, exceptions being the H^+ and OH^- ions, with mobilities of 36.25×10^{-4} and $20.50 \times 10^{-4}\,cm^2\,V^{-1}\,s^{-1}$, respectively.
2. *Electroosmotic flow* (EOF), consisting of the motion of the liquid along the surfaces of the electrolyte container. This EOF is based on the drag force that is exerted on the electrolyte by double-layer charge moving in an electric field. The double layer is a result of a change in space charge density close to container walls which become charged when they are in contact with electrolyte (e.g., a glass wall will carry

a negative charge in contact with an aqueous liquid at neutral pH). EOF can be switched on/off easily through switching of the voltages that establish the electric field. Similarly, switching of flows from and to different liquid lines is possible without mechanical valves, allowing complex sample and reagent manipulation. This *electrokinetic valving* concept has been exploited for the injection of minimized sample fractions in capillary electrophoresis chips to separate DNA fragments (Harrison et al., 1993). The liquid velocity v_{EOF} corresponding to the EOF can be described with an equation similar to that for electrophoresis, but with a different mobility, μ_{EOF}:

$$v_{EOF} = \mu_{EOF} E \tag{2}$$

where

$$\mu_{EOF} = -\frac{\varepsilon\zeta}{4\pi\eta} \tag{3}$$

in which η and ε are the viscosity and the dielectric constant of the liquid, respectively, and ζ is the zeta potential, that is the electric potential that arises at a defined position in the double layer. This potential strongly depends on pH and wall material. Typically, for an aqueous solution with a salt concentration of a few mM, the electroosmotic mobility in a Pyrex glass tube at pH 7 is ~$4.8 \times 10^{-4}\,cm^2\,V^{-1}\,s^{-1}$. For typical electric field values of a few hundred volts per centimeter, a linear liquid velocity of a few millimeters per second will be achieved.

An important advantage of the use of EOF to pump liquids in a microchannel network is that the velocity over the microchannel cross section is constant, in contrast to pressure-driven (Poisseuille) flow, which exhibits a parabolic velocity profile. EOF-based microreactors therefore are nearly ideal plug-flow reactors, with corresponding narrow residence time distribution, which improves reaction selectivity.

Although for separation methods like capillary electrophoresis EOF is often deliberately suppressed by specific wall coatings, in most practical cases, the species which are dissolved in an aqueous solution and which are relevant for the desired synthesis will be charged and therefore they will experience both an electrophoretic (of the dissolved species themselves) as well as an electroosmotic (of the solvent) driving force. Since the direction of EOF for aqueous solutions in a glass microchannel is toward the negative electrode, for a cation the electrophoretic and electroosmotic forces add up to a larger positive value, while for an anion the two forces are opposite and lead to a retardation and possibly even to a negative velocity with respect to the direction of EOF and cations. In any case, species of different mobility become separated in different zones, at least if they originally were introduced as a plug into the main solvent stream, as is the case in capillary

electrophoresis on a chip (Harrison et al., 1993). This concept has also been exploited in microreactors, in particular by researchers at Hull University in the United Kingdom (for literature references see below).

Spatial and temporal control of chemical reactions by electrokinetic principles relies on the possibility to direct reagents and products to or from selected points in a microchannel network, at specific times. An electrokinetic microfluidic network may be modeled as an electrical resistance network, using the well-known Kirchhoff voltage and current laws (Cummings et al., 2000; Fletcher et al., 1999, 2001, 2002; Qiao and Aluru, 2002), in which the flow rates are directly proportional to the electric currents. A pressure-driven microchannel network can be modeled with the same laws if they are rewritten in terms of hydraulic resistances and pressures and volume flows (Bula, 2009; Chatterjee and Aluru, 2005), but the electrokinetic case can be more complex if the local resistivity (and therewith the local electric field) changes due to electrophoretic separation and a phenomenon called *electromigration dispersion*. Such effects require the inclusion of the Kohlrausch's regulating function (Kohlrausch, 1897) in the model (Mikkers, 1999). We refer to the literature for more details about these phenomena and related effects like "stacking" which is often used in capillary electrophoresis to enhance separation. Deviations from the "ideal" uniform-resistivity-based network typically occur when a plug of an electrolyte with a resistivity largely different from the background electrolyte is injected in that background electrolyte. This would be analogous to a local variation in viscosity in pressure-driven flow, for example, for gas–liquid flow in a microchannel, or for injection of a highly viscous sample into a liquid chromatography column, leading to an instability called "viscous fingering" (De Malsche et al., 2009). That clean "switching" of flows in a simple Y-type microreactor inlet, using electrokinetic principles, is not as simple as it may seem, has recently been discussed in detail by MacInnes et al., who have shown that clean switching is difficult to achieve in practice, and that there is considerable contamination of each reagent supply channel with the other reagents (MacInnes et al., 2003). It has also been shown that the conductivity of the surface may play a significant role in electrokinetic flow principles (Fletcher et al., 2001) and that for extremely small channels, *nanochannels*, the situation becomes even more complex due to *electric double-layer overlap* (Sparreboom et al., 2009).

EOF has been applied as a pumping or mixing mechanism in microreactors (Fletcher et al., 2002). Mixing concepts include the introduction of two (or more, see Kohlheyer et al., 2005) parallel streams from a T- of Y-junction, where mixing at the low Reynolds numbers achieved occurs principally by interdiffusion of the two streams. This is a relatively slow process which may take tens of seconds to complete. Faster mixing can be achieved by injection of a sample of a specific composition via, for example, a double T-injector into a stream of liquid with a different composition.

Mixing speed is controlled by the width of the injected plug, and will be much faster than in the parallel-stream case (Fletcher et al., 2002).

Electrophoretic concepts have also been used for mixing purposes, for cases where the two reagents to be mixed have a different mobility, for example, applied in Wittig chemistry (Skelton et al., 2001a). Using electrophoretic principles to generate controlled concentration gradients of reagent streams, again in a Wittig synthesis, it was found possible to control the *cis* (*Z*) to *trans* (*E*) isomeric ratio in the product in the range 0.57–5.21, compared to a traditional batch method which gave a Z/E ratio in the range 2.8–3.0 (Skelton et al., 2001b). Several other examples of synthetic reactions carried out in a microreactor under electroosmotic or electrophoretic control, or both, have been reviewed by Fletcher et al. (2002). It was also demonstrated that similar principles can be applied with organic solvents, as long as they have sufficient polarity (Salimi-Moosavi et al., 1997). Watts et al. have shown that peptides may be prepared in quantitative conversion in a microreactor under electrokinetic control, with an increase in reaction efficiency compared with the traditional batch method. This increase was found to be due to an electrochemical effect (Watts et al., 2004). Finally, one specific other application of differential electrophoretic mobility is the selective control of product detection times in capillary electrophoresis in a method called *electrophoretically mediated microanalysis* (Bao and Regnier, 1992; Burke and Regnier, 2001).

In a previous section the concept of (simulated) moving bed chromatography was briefly discussed. Electrophoresis shows a resemblance to true moving bed chromatography, because negative and positive ions become separated and move relative to one another in opposite directions in an electric field. For species which have a charge of the same sign, a properly directed EOF, which can be tuned by changing the surface charge via an external electrode (Culbertson and Jorgenson, 1999; Schasfoort et al., 1999), via EOF modifiers or dynamic wall coating (Kaniansky et al., 1999; Melanson et al., 2001) or via a permanent surface coating (Revermann et al., 2008), or a well-tuned co- or countercurrent pressure-driven flow (Culbertson and Jorgenson, 1994) may establish the correct relative velocities for an electrophoretic moving-bed-like process. In a number of publications Thome and Ivory have described the continuous fractionation of enantiomer pairs using such an electrophoretic analog of moving bed chromatography (Thome and Ivory, 2002, 2006, 2007), using an industrial scale vortex-stabilized electrophoresis instrument. The concept is shown in Figure 24 (Thome and Ivory, 2007). It would be ideally suited for downscaling, as is the case for all electrophoretic principles, and similarly ideal for a downstream work-up method coupled to a (electrokinetically controlled) microreactor, but as far as we know this has not been attempted yet.

The methods described above all deal with direct current electroosmosis and electrophoresis. If electroosmosis is used with a time-periodic

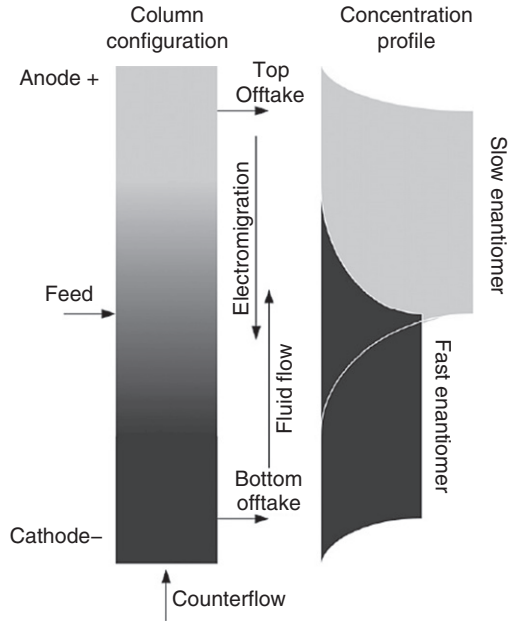

Figure 24 Electrophoretic moving bed separation of enantiomers. The downward movement of the enantiomers by electromigration is counteracted by a fluid flow upward. The fast enantiomer still has a net migration to the bottom outlet, while the slower enantiomer is pushed toward the top outlet (reprinted from Thome and Ivory, 2007, with permission from Elsevier).

electric field over a liquid volume, special effects can be generated. The first obvious effect is enhanced species mixing. Mixing is always an issue in microfluidic reactors, and electric fields in liquids may assist in this process in several ways. Above we have already discussed the application of electrophoresis to mix charged species without actual liquid movement. EOF induced by an unsteady electric field was experimentally shown to improve mixing (Oddy et al., 2001; Qian and Bau, 2002). The difference between the approaches of Oddy et al. and Qian and Bau is that in the first a flow instability, observed in sinusoidally oscillating, electroosmotic channel flow is used to generate stretching and folding of stream lines, while in the second periodic alternations of local ζ potentials is applied to induce chaotic advection (see also Chang and Yang, 2009). Spatial and temporal control of the ζ potential can be achieved by imposing an electric field perpendicular to the wall liquid, using electrodes embedded in the insulator wall (Schasfoort et al., 1999; van der Wouden et al., 2005).

It has also been demonstrated that nonuniform AC electric fields generated by neighboring coplanar microelectrodes produce a steady fluid flow in electrolytes (see Green et al., 2002, and refs. therein). The

liquid moves from high-field strength regions on electrode edges to the surface of the electrodes, with the highest velocity found at the edge. The velocity depends on frequency and amplitude of the applied electric field, goes to zero at high- and low-frequency limits and has a maximum at a frequency that depends on the electrolyte conductivity (Green et al., 2000). Microfluidic devices with incorporated arrays of nonuniformly sized embedded electrodes, subjected to an AC field, were shown to generate a bulk fluid motion (Brown, 2000; Studer et al., 2002). The mechanism responsible for the liquid flow is the interaction of the tangential component of the electric field and the induced charge in the diffuse double layer on the electrode surface (Green et al., 2002), and will work best if an asymmetry is created in the coplanar electrode pattern, see Figure 25 (Brown, 2000). Typical liquid velocities that can be achieved with the method are 1 mm per second, at typical voltages of 1–10 V (rms).

4.2 Positioning and trapping of particles and molecules

AC electroosmosis as discussed in the previous section has not been used much as a pumping mechanism in microreactors, but the effect has been shown to be useful in (bio)particle manipulation, for example, in the work on an electrokinetic bioprocessor used for concentrating cells and molecules in a microfluidic system (Wong et al., 2004). In this device, the flow field generated by AC electroosmosis transports particles to regions near the electrode surface, where electrophoretic and *dielectrophoretic* forces, which are effective in short range, take over, and trap the cells and molecules. The concentration of biological objects in a large range of sizes, including bacteria, λ-phage DNA, and single-stranded DNA fragments with a radius of gyration of 3 nm, was demonstrated.

DEP is based on a force exerted on a dielectric particle by a nonuniform electric field. The strength of the force depends on the electrical properties

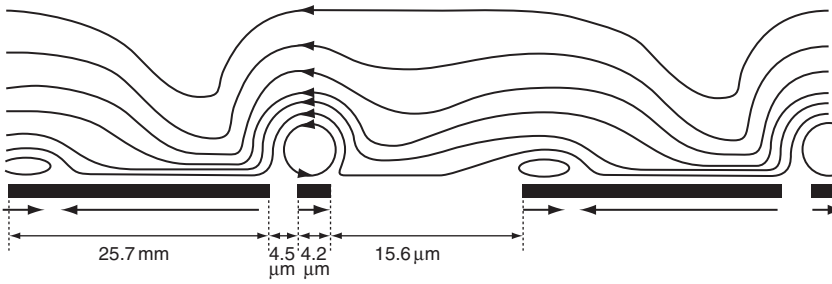

Figure 25 Predicted flow profile over asymmetric pairs of electrodes (from Brown, 2000; reprinted with permission. Copyright 2000 by the American Physical Society).

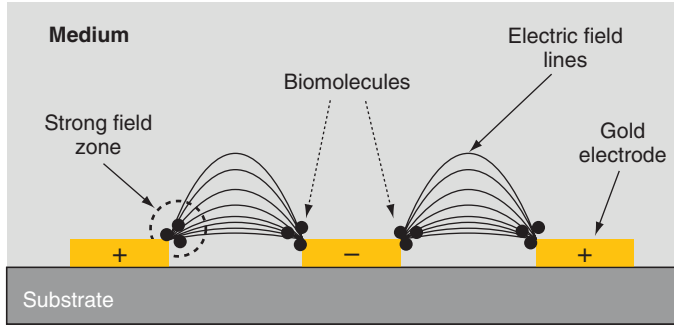

Figure 26 The principle of positive DEP, for biomolecules (from Luo et al., 2006; reprinted with permission from Elsevier).

of medium and particle, on particle shape and size, and on electric field frequency. DEP can be either *positive* (*p*-DEP), which is when the particle is attracted to a region of higher electric field because its permittivity exceeds that of the suspension medium (see Figure 26, Luo et al., 2006), or *negative* (n-DEP), attracting it to lower electric field if the permittivity of the medium is higher than that of the particle (Pohl, 1978). DEP is typically observed for particles with diameters of 1–1000 μm, but it is possible to apply it for smaller particles, and even biomolecules, as was shown in the work of Wong et al. (2004). For more accurate trapping of nanoscale objects like bovine serum albumin and antibody molecules (these have a size in the range of ~10–14 nm), Luo et al. have developed DEP with an array of nanoelectrodes with a width of 60 nm and a period of 380 nm, by which the EOF that disturbs trapping, is suppressed, and furthermore the required voltage is reduced by a factor of five in comparison with a microelectrode configuration (Luo et al., 2006). Although this has not been discussed in the work of Luo et al., the dimensions of the electrodes should not be very small in comparison with the microfluidic channel height (Markarian et al., 2003).

DEP can be used to create regular patterns of particles on a surface or in a microfluidic channel. For example, two-dimensional (2D) patterns of polystyrene latex microbeads were fabricated on glass substrates using n-DEP, and the line- and grid-patterned microparticles, which formed due to the repulsive force of this n-DEP, were covalently bound on the substrate via cross-linking agents (Suzuki et al., 2004). In this work, interdigitated microelectrodes were incorporated into a fluidic channel in order to direct the particles into very specific patterns.

Regular pattern formation in a particle deposit can occur spontaneously, through a self-assembly process that is based on the adhesive or repulsive interaction between particles and between particles and a surface. Electric fields may assist in pattern formation, via the forces between particles caused by their polarization in the DEP process, but

also through electrophoretic (Trau et al., 1996) or electroosmotic transport (Solomentsev et al., 1997) of the medium or the particles in it along or toward a surface. Furthermore, to actively control the formation of colloidal crystals inside microchannels, a combination of electrocapillary forces and solvent evaporation was used (Shiu et al., 2004). Electrocapillary forces are capable of controlling fluid motion in three-dimensional (3D) structures, and the resulting well-ordered 3D patterns of particles could be very interesting for the field of catalysis in general, and catalytic microreactors in particular. Ordered packed beds would have a lower residence time distribution (in analogy with a lower theoretical plate height in chromatographic applications, see De Malsche et al., 2007) and therewith may give an improved reaction product selectivity.

Electroimmobilization of different enzymes in a microfluidic device has been described as a means to perform multistep reactions (Astorga-Wells et al., 2004). The procedure consists in first capturing target molecules by balancing opposing hydrodynamic (i.e., pressure-driven flow) and electric forces (i.e., EOF), after which a second medium, carrying enzymes or other reagents, is injected into the system and brought into contact with the target molecules to allow them to react. Disconnecting the electric field reverses immobilization and allows to collect the products at the outlet of the device. Examples of reactions that were carried out in this way are reduction, alkylation, and trypsin digestion of proteins. A similar concept has been used to separate peptides (Astorga-Wells et al., 2005).

CNTs and CNFs have already been discussed several times in this chapter. For applications in the microreactor field, they have become important as catalyst support because of their corrosion resistance to acids and bases, their high surface area, and the possibility to tune their surface chemistry (see De Jong and Geus, 2000 for a review). CVD is the most popular method of producing these carbon nanostructures, due to both the large-scale production feasibility and the possibility of controlling length, diameter, orientation, and growth locations of the structures. Typically, they grow from metal nanoparticles like Fe, Ni, Co, or their alloys, and then develop into 5–20 nm thick and a few to tens of micrometers long multiwalled nanotubes. Their electric behavior can vary from semiconducting to metallic.

However, a serious issue for device integration with CNTs is posed by the inability to control whether the tubes or fibers are semiconducting, semimetallic, or metallic. This aspect will also play a role if carbon nanostructures are used as a catalyst support. Except for a selective destruction of metallic tubes (Collins et al., 2001) an interesting method to separate metallic from semiconducting CNTs is the use of AC DEP. This is done by bringing a suspension of the tubes in contact with a microelectrode array. Due to the different dielectric constant of the species with respect to the

solvent, an opposite movement of metallic and semiconducting tubes arises along the electric field gradient generated by the electrode array (Krupke et al., 2003). Subsequent work has shown that sorting improves with increasing AC frequency (Krupke et al., 2004). This dielectrophoretic separation concept has recently been implemented in a microfluidic setup, where the separation is facilitated by two parallel streams of liquid, where the metallic tubes are subjected to a significantly larger dielectrophoretic force perpendicular to the flow direction and drawn into the second stream, while the semiconducting tubes remain in the first stream (Shin et al., 2008). This approach, which is very similar to earlier work based on dielectrophoretic field-flow fractionation (Peng et al., 2006), significantly increases throughput. The final goal of this work is the fabrication of nanoelectronic devices, but the use of such concepts can become very valuable for manipulation and positioning of catalytic nanoparticles in future. For example, positive DEP was used to interface CNTs and catalytic Pd to realize a H_2 gas sensor (Suehiro et al., 2007). CNTs were either trapped alone, or simultaneously with Pd nanoparticles (giving CNTs modified with Pd nanoparticles), on Pd electrodes.

Recently reports have appeared in literature about the control of *single* nanoscale objects in liquids by electric fields. Control of micrometer-scale objects had been reported earlier already, but for smaller objects special care has to be taken to compensate for the Brownian motion of the particles. Cohen et al. (Cohen, 2005; Cohen and Moerner, 2005) created an electrophoretic trap which creates arbitrary 2D force fields for individual nanoscale objects in solution, couples fluorescence microscopy with digital particle tracking, and real-time feedback to generate a position-dependent electrophoretic force on a single nanoparticle. The control of position for a 20 nm particle was within a few microns. It is stated that positional control of a single fluorophore is fundamentally limited by the finite rate of photon detection. State of the art would allow the control of a typical fluorophore within 1 μm, if sufficient electric field could be generated, which would require an electrode pattern with an interelectrode gap on the order of 3 μm. This is indeed possible with current photolithographic techniques. The authors have demonstrated trapping and manipulation of single virus particles, lipid vesicles, and fluorescent semiconductor nanocrystals (Cohen and Moerner, 2006). This work could also become very relevant for the study of the chemical reactivity of single surface-modified beads, single catalyst particles, and single enzymes.

As a final demonstration of new technological achievements, it was recently also demonstrated that *gas molecules* can be trapped in an electric field on a chip (Meek et al., 2009). Manipulating a packet of ions in a vacuum is quite common practice in mass spectrometric instrumentation, where ions can be collected and analyzed in, for example, ion traps and

collision cells, and their flow can be steered by electrostatic lenses (and magnetic fields) through time-of-flight detectors and other sophisticated ion separators and analyzers. In the work by Meek et al., though, CO molecules, loaded directly from a supersonic beam, were confined in tubular electric fields of 20 μm in diameter and centered 25 μm above a chip. These field traps move with the molecular beam at a velocity of several hundred $m\,s^{-1}$ and can hold molecules for a certain time, and subsequently release them off the chip for detection. The authors claim that this methodology is applicable to a wide variety of polar molecules, and enables "the creation of a gas-phase molecular laboratory on a chip" (Meek et al., 2009). Although these authors discuss their results mainly in the light of quantum optic and solid-state technology (quantum computing), one can foresee applications for chemical synthesis as well, if such microstructures can be reconfigured for the manipulation and recombination of small packages of different molecules, in combination with fast spectroscopic methods to study chemistry.

4.3 Electrowetting-on-dielectric

The use of droplets as microreactors has been discussed already many years ago (Pileni, 1993), but the combination with microfluidic networks which give control over individual droplets and their composition has brought upon a completely new field of research, which, since it works with discrete liquid packets, may also be referred to as *digital microfluidics*. Digital microfluidics shows a clear analogy with traditional benchtop protocols, and a wide range of established chemical protocols can seamlessly be transferred to a picoliter to nanoliter droplet format. *Electrowetting*, that is, the change in surface tension caused by an electric field (Berge, 1993), DEP, and immiscible liquids in pressure-driven flow are the three most commonly used principles used to generate and manipulate the droplets in a digital microfluidic device.

EWOD is used to control the flow of liquid droplets on a surface or in a channel and works both with droplets in air, with droplets of a liquid immiscible with the surrounding liquid (e.g., water–oil combinations), and even with air bubbles in a liquid (Zhao and Cho, 2007). Typically, in an electrowetting device, a voltage of 50–100 V is applied across a 1-μm-thick insulator, which causes the contact angle of an aqueous solution on a hydrophobic surface to decrease from ~115° to ~75°. But by using a very thin (70 nm) and high dielectric constant (~180) material, only 15 V are needed to give about the same contact angle change (Moon, 2002). The theory of EWOD have been discussed in detail in recent reviews (Mugele, 2009; Mugele and Baret, 2005), and for an overview of applications of droplet microfluidics, including EWOD, we refer to another recent review (Teh et al., 2008).

Here we want to highlight the use of EWOD in microfluidic networks or on surfaces with embedded electrodes as microreactors. Several research groups have worked on this concept, and each group has its own favorite design, operation regime or application field (Pollack et al., 2002; Taniguchi et al., 2002). EWOD-based mixers have been described that work either on the fast displacement of droplets on an array of electrodes and the accompanying internal flow in the droplet generated by the rolling movement (Paik et al., 2003), or on the periodic change of contact angle of the droplet (Mugele et al., 2006; Nichols and Gardeniers, 2007), which leads to stretching and relaxation of the droplet, and therewith to a sort of "shaking" effect that speeds up mixing. Although a fundamental explanation for the observed behavior is still lacking, it was found possible to mix an enzyme with its substrate in a time as short as 15 ms with EWOD at an optimal AC frequency of 750 Hz, in a study on the pre-steady-state enzyme kinetics of a specific phosphatase (Nichols and Gardeniers, 2007). The reaction mixture was then rapidly quenched with an acid by the same principle, and subsequently mixed with a matrix solution in order to prepare it for MALDI-TOF (Matrix Assisted Laser Desorption Ionization Time-of-flight) mass spectrometry, a method that, because of its off-line character, matches perfectly with digital microfluidics (Wheeler et al., 2004).

4.4 Special effects

In this section we would like to briefly describe a number of less developed and in some cases unexplained ideas and phenomena based on electric fields, which have been or may be used in combination with chemical (micro)reactors. They are posed here as possible suggestions for further research.

4.4.1 Electric wind

The first principle is that of *electric wind* (or ion wind, ionic wind, or coronal wind), the earliest report of which was already made in 1709 by Hauksbee (Robinson 1962). Since electric charge resides entirely on the external surface of a conductor and concentrates around sharp points and edges, the electric field on a point or edge is much higher than that on a flat or smooth surface. When this field exceeds a certain strength, known as the corona discharge inception voltage gradient, it ionizes the air close to the tip. The ionized air molecules have the same polarity as the tip, so that they are repelled and create an electric "wind" in a direction away from the tip.

One of the applications of electric wind is in aerodynamics, in which field it has been an important objective to modify airflow around an obstacle in order to reduce drag. The advantage of flow control by an

electrohydrodynamic concept that directly converts electrical energy into mechanical energy is that no moving mechanical parts are involved and a very short response time, because of the electric control, is established (Magnier et al., 2007; Moreau, 2007). Another application is in spacecraft propulsion, where an *ion thruster* creates thrust by accelerating ions (Lerner, 2000). Although the thrust created in ion thrusters is quite small compared to chemical rockets, a high propellant efficiency is obtained because of the very limited propellant consumption. Electric wind also helps in the enhancement of heat transfer (Kalman and Sher, 2001) and was suggested and tested as a concept for cooling of microelectronic circuits (Go et al., 2007) where thin-film electrode patterns of a stable material like diamond with gaps of several micrometers were shown to be particularly useful (Go et al., 2009). Experimental work demonstrated a more than twofold enhancement of the local heat transfer coefficient with ionization combined with typical externally forced flow conditions (Go et al., 2007). This concept, and several other principles of *microscale thermal transport* such as pool boiling heat transfer enhancement and convective flow boiling in microchannels, which may become relevant for implementation in microreaction technology as well, have recently been reviewed (Garimella and Liu, 2009).

A direct application to chemical process technology of the principle of electric wind is in *electrostatic precipitators* (Leonard et al.,1983) and *electrocyclones* for size separation of particles in powder technology (Nenu et al., 2009). Electrostatic precipitators applied to exhaust gas cleaning have recently been reviewed (Jaworek et al., 2007). A particularly interesting development is that of a small electrocyclone with a diameter of 75 mm (Shrimpton and Crane, 2001). With this device it was shown that the separation quality of the smallest size particles with a diameter below 38 μm doubled upon application of the electric wind. Later experiments performed with submicron silica particles demonstrated that classification of such particles is possible by use of an electrical hydrocyclone (Nenu et al., 2009).

4.4.2 Electric swing adsorption

A very recent development, with the objective of reusing greenhouse gases like CO_2, is *electric swing adsorption* (Moon and Shim, 2006). As an alternative to pressure swing adsorption, which utilizes a vacuum, or thermal swing adsorption, which applies a hot inert gas, to recover a gas that was separated from a mixture by selective adsorption on a specially selected material (like a zeolite), electric swing adsorption utilizes a direct electrical current to heat the material, so that the gas desorbs quicker and with lower energy consumption. The feasibility of the concept for capturing CO_2 from flue gases with 3.5% CO_2 from natural gas power stations was studied,

and it was found that an adsorbent consisting for 70% of zeolite and for 30% of a conducting binder material can give a concentrated stream with 80% CO_2 with an energy consumption of 2.04 GJ per ton of CO_2 (Grande et al., 2009). This work indicates that electric swing adsorption may become an interesting CO_2 capture technology.

4.4.3 Pulsed electric fields

Pulsed electric fields are used in food preservation to inhibit microorganisms in foods without significant loss of flavor, color, taste, and nutrients. The treatment generates a very short (microseconds) but high electric current pulse through the food. The topic has recently been reviewed, including the fundamental mechanisms of food preservation (Min et al., 2007). The main mechanisms for microbial inhibition are structural damaging of cells, in particular cell membranes, due to a number of mechanisms related to cell stress and fatigue, and inactivation of enzymes due to association or dissociation of functional groups, movement of charged chains, and changes in the alignment of helices.

A peculiar recent report is that in which the application of an AC high voltage to accelerate wine aging is discussed (Zeng et al., 2008). The optimum treatment was found to be with an electric field of 600 V cm^{-1} for 3 min. Several analysis techniques were used to clarify the differences between treated and untreated wine samples, and it was found that the amount of higher alcohols and aldehydes in volatile compounds decreased significantly while the amount of some of the esters and free amino acids slightly increased. A mechanism that may be responsible for the formation of the free amino acids is protein degradation, but otherwise no explanations have been given for the effect of the AC electric field.

4.4.4 Electrospray

Electrospraying is a concept in which an electric field is applied between a liquid outlet and an object at some distance from the outlet. The liquid becomes dispersed and develops into a very fine aerosol because droplets break up due to a Rayleigh instability, that is, the phenomenon that a thin beam of a liquid in a gas becomes unstable at a certain length and breaks up into droplets, which effect is enhanced by an electric field on the liquid (Rayleigh, 1882). A related concept that is used very frequently to generate ions that can be separated in a mass spectrometer is *electrospray ionization* (ESI). Here a high voltage is applied to a liquid supplied through a nozzle (e.g., a small glass capillary). The liquid forms a so-called Taylor cone, at which apex droplets break up into a fine spray with smaller and smaller droplets because of radial dispersion due to Coulomb repulsion in combination with solvent evaporation, until finally all the solvent is evaporated and all the solutes have become ionized and can enter the

mass spectrometer inlet to become separated and detected. ESI has been reviewed many times in literature, and has become a very valuable concept for coupling microreactors and other (analytical) microdevices to a mass spectrometer (Le Gac and van den Berg, 2009).

Electrospray has been used for many different applications, such as the deposition of paints and coatings on metal surfaces and the deposition of metal nanoparticles and biomolecules on biosensor surfaces, and in a miniaturized version also as a propulsion mechanism in microsatellites (see also the section on electric wind). One particularly interesting application is in *fuel atomization*, that is, a finer fuel aerosol and atomization will give a higher combustion efficiency and less pollutant emission, which is caused by the effect that finer droplets increase the total surface area on which combustion can start (Lehr and Hiller, 1993).

There has been a claim of another useful effect of electric fields on fuels, that is, an electric charge on a fuel tube is said to reduce fuel viscosity, so that fuel injectors will create smaller droplets, which enables cleaner and more efficient combustion. The principle is that molecules in the fuel become charged and aggregate, reducing their overall surface area, therewith decreasing the viscosity (Tao et al., 2008). The paper by Tao et al. received serious criticism, where the criticism is that, although the application of an electric field might indeed reduce fuel viscosity and lead to finer atomization, there is no proof that finer atomization would improve combustion efficiency by 20%, while it is also stated that the earlier "claims and conclusions violate the first law of thermodynamics" (Gulder, 2009). This, as might be expected, is rebutted by the authors of the first paper (Tao et al., 2009). Nevertheless, this idea may become a topic with a high impact, and surely deserves further research.

5. ELECTRONIC CONTROL OF REACTIONS AT SURFACES

5.1 Adsorption–desorption controlled by electrical fields

Electric fields at field emitter tips, as discussed before, are typically on the order of $10\,\mathrm{V\,nm^{-1}}$. This is in the same range as the electrostatic fields that are present in zeolite cages (see below) and at the interface of electrode and electrolyte interface. Since these fields are all of the same order as the fields inside atoms and molecules, they are strong enough to induce the rearrangement of electronic orbitals of atoms and molecules. It is therefore expected that it should be feasible to stimulate chemistry with such electric fields.

In this section we are particularly interested in *field-induced adsorption/desorption* (Kreuzer, 2004). In the review by Kreuzer, electric field effects are classified either as physical, for fields below $10\,\mathrm{V\,nm^{-1}}$ which mainly

give rise to polarization, or as chemical, for fields above 10 V nm^{-1}, which give rise to such a level of distortion of electronic orbitals of atoms or molecules that new bonds may form. Far from the surface and in the absence of an electric field, the atomic orbitals of two atoms hybridize into two molecular orbitals, a lower bonding and a higher (empty) antibonding orbital. As the molecule approaches the metal surface, additional hybridization with the conduction electrons occurs, leading to shifts and broadening of these orbitals, so that the antibonding orbital becomes partially occupied, resulting in bonding to the surface. An electric field pointing away from the surface adds a potential energy for electrons outside the metal, which raises the atomic levels of atoms A and B, resulting in a rearrangement of the molecular orbitals. For this situation, the antibonding orbital becomes empty again, and the surface bond probably weakens. At a field strength where the bonding orbital is lifted above the metal Fermi level, this orbital will also drain, and field-induced dissociation will occur.

This principle has been applied in *field ion microscopy* (FIM), in which a (pulsed) electric field generated by a sharp metal tip allows the investigation of the field effect on chemical reactions (Block, 1963). Typically, the potential at the tip is *positive* and generates a field close to it of ~10 V nm^{-1}, the chamber in which the tip is applied is at high vacuum, and the tip is cooled to temperatures of ca. 20–80 K. Quite similar to FIM is *field emission microscopy* (FEM), which also applies a sharp metal tip but at a large *negative* potential, giving an electric field near the tip on the order of ~10 V nm^{-1}, high enough for field emission of electrons to occur. Both these techniques are valuable for studies of the interaction of gases with catalyst surfaces, as has been shown recently in an investigation of the interaction of carbon monoxide and oxygen with gold (McEwen and Gaspard, 2006). In this work a field-dependent kinetic model based on the Langmuir–Hinshelwood mechanism was constructed to show that dissociative adsorption of oxygen on gold occurs only below a negative critical electric field value, while binding of CO on gold is enhanced for positive field values. Although the experimental conditions are far from the ones in practical catalytic chemistry (on the surface of a metallic tip the electric field varies according to the local radius of curvature, leading to spatial differences in adsorption and desorption of molecules, while also pressure and temperature are significantly different), this research can still give important clues about the surface processes occurring on a catalytic particle (like a Au nanoparticle with a diameter of a few nm) on a specific support (see Figure 27). The charged metal tips not only mimic the well-known (electronic) metal–support interaction in catalysis (Yoshitake and Iwasawa, 1992), but also modify the pressure of the gases close to the surface of the catalyst particle due to the polarizability and the electric dipole of gas molecules. Using the equilibrium statistical mechanics of diatomic molecules in an electric field, the effective potential of the molecules at 300 K can be approximated by a quadratic

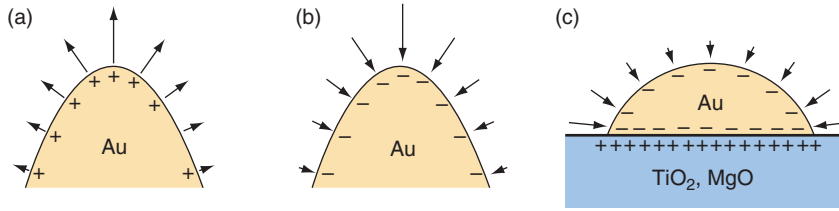

Figure 27 (a) positively charged gold tip in FIM, (b) negatively charged gold tip in FEM, and (c) negatively charged gold cluster on an oxide solid substrate (from McEwen and Gaspard, 2006; reprinted with permission. Copyright 2006, American Institute of Physics).

function of the field, and from that the dependence of the pressure of a specific molecule on the electric field F can be approximated by a function of the general form:

$$P(F) \cong P(0)\exp\{\beta u_{\text{eff}}\} \tag{4}$$

where $\beta = (k_B T)^{-1}$, with k_B Boltzmann's constant, βu_{eff} the mentioned effective potential of the molecule, and $P(0)$ the pressure at a position where the electric field can be supposed to vanish. In the cited work of McEwen and Gaspard, the effective potentials of O_2 and CO are 0.022 and 0.028 $(\text{V nm}^{-1})^{-2}\, F^2$, respectively, which at a tip electric field of 10 V nm^{-1} gives pressure enhancements of factors 9.5 and 17, respectively (McEwen and Gaspard, 2006).

Above we already mentioned that the electric fields achievable at a metal tip to which a voltage is applied can be in the same range as the electrostatic fields that are present in zeolite cages, for example, the electrical fields present on unshielded alkali ions in zeolite Y are estimated to be on the order of 3–10 V nm^{-1} (Blatter et al., 1994). Such large fields stabilize charge-transfer states of properly oriented colliding hydrocarbon and oxygen pairs, so that reactions between them can be initiated at the low energies of visible photons or even by mild heating (Frei, 2006). Similarly, electrostatic fields play a role in the ability of a *metal-organic framework* (MOF) material to separate gas mixtures (Yang and Zhong, 2006). The selective gas adsorption in an MOF is related to both the pore size and the interactions between adsorbed molecules and the pore walls. If the MOF has surfaces with high electrostatic fields or field gradients, the adsorption of molecules with a high dipole or quadrupole moment, respectively, will be enhanced, for example, in the MOF of type HKUST-1 (Li et al., 2009).

A question that arises is whether one can modify the electrostatic fields (or their gradients) around active sites in zeolite cages or around the pores in an MOF, by applying an *external field*. As far as we know experiments of this kind have not been reported, but a possible experimental configuration to do so is a capacitor in which the zeolite is sandwiched between two

charged electrodes of a conductor (which should preferably be catalytically inactive, excluding most of the noble metals). A way to analyze the local intracrystalline electric field gradients in the zeolite and their possible modification by external electric fields is NMR of quadrupole spins, like those of adsorbed ^{131}Xe (Millot et al., 2001). It is doubtful whether the zeolite or MOF in the mentioned capacitor structure can withstand the electric fields required to get a significant effect on the catalytic activity. For example, the breakdown field strength of dense silicon dioxide, one of the most reliable insulators available in microelectronics, is ~1 V nm^{-1}, and breakdown of zeolites of MOFs will most likely occur at lower fields than this. This is why in our laboratory we are studying configurations based on insulated nanoneedles, at the tips of which the electric field will be significantly enhanced.

The field of fine and pharmaceutical chemistry, where the desired production amounts are in kilograms rather than in tons, would benefit considerably from the development of versatile process chemistries, carried out in relatively small generic production units that can be tuned to a range of different products. An example of a versatile "microreactor" is a microorganism of which the product can be tuned by engineered genetic changes that alter the metabolic processes of the organism in such a way that it produces a desired chemical. The key actors in this are the different enzymes which are expressed by the microorganism and which perform the required biocatalysis on very specific feed molecules to deliver the desired product molecules with extremely high selectivity, for example, as a single enantiomer. Enzymes in living cells are often not present free in solution but immobilized in the lipid membranes of cell organelles or of the cell outer membrane. It is difficult to replicate membrane immobilization outside of a cell, in a technical device, which is why for industrially relevant enzymes immobilization strategies have been developed based either on support binding (usually involving covalent bonds, for example, to a resin, a biopolymer or a mesoporous silica), entrapment (in a gel lattice), or cross-linking of enzyme aggregates or crystals to prepare carrierless particles (Sheldon, 2007).

For reasons of fouling or deactivation, it may be desirable to be able to replace immobilized enzymes in time, and for this a programmable way of adsorption and release of enzymes would be very welcome. An example of this is the use of a 4 nm thin polymer film that can be thermally switched between a hydrophilic (swollen) state at 20 °C and a more hydrophobic protein-adsorbing (collapsed) state at 48 °C, integrated into a micro hotplate with fast heating options so that a protein monolayer can be adsorbed and released within 1 s (Huber et al., 2003).

The application of heat to enzymes is not always desired; furthermore, it may turn out to be difficult to localize the heat. Electric fields have an advantage in this respect, since they can be locally applied by design of

electrode configurations. Besides the concepts which were already mentioned earlier in which electric fields are applied to transport molecules or particles to a desired location, or trap them at a specific location, there are also ways to control the adsorption of molecules from solution on a specific surface.

Two principles exist by which electric fields can control molecular adsorption on a surface. The first is based on a change in surface wetting properties, as was discussed in a previous section, where EWOD was applied to switch from a hydrophilic to a hydrophobic state and *vice versa*. The second relies on changing the surface charge density, for example, on a metal electrode in contact with an electrolyte, or changing the ζ potential, by applying an external electric field on electrodes embedded in an insulator surface on which one desires to change the affinity. Experiments involving the adsorption of organic molecules at a solid surface have shown strong capacitance changes in the electric system in which the solid surface was included, which changes are associated with phase transitions in the adsorbed layer between gas-like layers, disordered and ordered physisorbed layers, and chemisorbed layers (Van Krieken and Buess-Herman, 1999). The concept of changing the ζ potential on a surface arranged in a field-effect transistor (FET) configuration by a *gate potential* was discussed in the section on EOF as a method to control that flow, but it should also be possible to control in similar manner the (reversible) adsorption of molecules, especially of molecules which have a charge or a dipole. The effect is very sensitive to the pH of the electrolyte with which the surface is in contact, and typically the largest effect of the *field-effect flow control* principle occurs close to the pK value of the surface of interest (Schasfoort et al., 1999; van der Wouden et al., 2005). This may prohibit the use of the concept for enzyme immobilization because also the mobility and solubility of proteins is very much pH dependent. Attempts in our laboratory (Nichols and Gardeniers, 2006) to use field-effect control of protein adsorption were unsuccessful, which may have been due to the problem of balancing the charge on the surface (controlled by the pH, ionic strength, and both the electric fields along and perpendicular to the surface) with the charge on the protein (controlled mainly by pH, and the choice of protein). Furthermore, in a theoretical study on electrostatic contributions to the entropy and energy of protein adsorption (Roth et al., 1998) it was shown that the attractive free energy is very strong at short range. The protein was modeled as a colloidal particle, with an electric double layer that starts to overlap with the electric double layer of the surface at short range, leading to a significant entropic effect due to ion transport from the double layers to the bulk of the solution. This (positive) entropic effect is said to dominate the free energy of adsorption. However, this effect very much depends on the matching of charges on the protein and on the wall, and in some cases this may even lead to a

repulsive force between protein and wall (Roth et al., 1998). Control seems therefore to be difficult or at least unpredictable. In addition, there is also always a risk that, due to the distortion of the ionic mantle around a protein molecule by a strong electric field, particularly at high protein concentrations, the protein solution becomes instable and starts to aggregate or precipitate, like it is the case for sols that may become destabilized by a change in ionic strength.

Probably, a combination of electrostatic effects (tuning the charge on a surface) and wetting effects is a better concept to control *reversible* and *nonspecific* adsorption of proteins. Proteins and other biomolecules in aqueous solutions tend to nonspecifically (i.e., not via their active bonding site) adsorb onto hydrophobic surfaces, but as mentioned above they can also become adsorbed through electrostatic attractions. It was shown that protein adsorption in an EWOD configuration could be minimized by limiting the time during which no potential is applied (which is the nonwetting i.e., hydrophobic state) and through choice of solution pH and electrode polarity (Yoon and Garrell, 2003). In another study, the adsorption kinetics of human serum albumin and horse heart cytochrome *c* under the influence of an electric field, from aqueous solution onto an indium tin oxide (ITO) electrode were investigated, with the aim of producing a surface-immobilized protein layer of tailored structural properties (Brusatori et al., 2003). With the aid of optical waveguide light-mode spectroscopy, it was found that adsorption rates changed according to the charge of the proteins in relation to the applied potential, but depended on the chosen buffer. The rate of adsorption at high surface density increased with the voltage for both studied proteins, which effect was more pronounced in water than in a HEPES buffer solution. This effect was attributed to contact between electrode and protein patches of complementary charge, leading to more oriented and more efficiently packed (multi)layer formation. It is important also to note that the metalloprotein azurin, entrapped on a silicon dioxide surface in-between metal electrodes of 1 μm width and with a gap of 1 μm, keeps its native configuration up to electric fields of 10^{-3}–10^{-2} V nm^{-1} (Pompa et al., 2005).

As a final topic in this section we would like to discuss a study aimed at the development of protein microarrays (i.e., planar substrates with regular spots with immobilized proteins of which the interaction with specific molecular probes or cells in solution is tested), in which an electrochemical switching strategy was implemented in order to modify surface properties (Tang et al., 2006). An ITO-based microelectrode array was uniformly coated with a protein-resistant polymer, poly-(L-lysine)-grafted-poly(ethylene glycol) (PLL-g-PEG). The electrical field induced by microelectrodes electrochemically removes the PLL-g-PEG adlayer from conductive areas, while the surrounding insulating surface is unaffected

and remains protein resistant. The unprotected microelectrodes are then surface functionalized with the desired biomolecules such as DNA, proteins, or lipid vesicles with membrane proteins.

5.2 Control of the activity of adsorbed molecules

Besides the control of the adsorption and desorption of molecules on a surface, an exciting topic is tuning of the *orientation* and the *activity of adsorbed molecules* by an electric field. For organic molecular layers adsorbed on electrodes, it was found that after the initial adsorption, a sufficiently high (positive) potential leads to orientation of the molecules, where the molecular dipoles align with the electric field so that adsorbate–adsorbate interactions are increased (Han et al., 2004; Pronkin and Wandlowski, 2003). For the zwitterionic molecule *p*-aminobenzoic acid (PABA) on an Ag(111) electrode surface also a potential-dependent orientation effect was observed, using infrared–visible sum frequency generation spectroscopy and electrochemical capacitance and CV measurements (Schultz and Gewirth, 2005). It was found that PABA switches orientation with the charge on the electrode surface, orienting one way for potentials above the potential of zero charge, and the other way below that potential, an effect that depends on pH.

While in the mentioned work on PABA on a charged silver electrode also the adsorption degree of the molecules was controlled by surface charge, Lahann et al. showed a concept in which molecules immobilized as a low-density self-assembled monolayer on a gold surface were electrically stimulated to undergo conformational transitions between a hydrophilic and a hydrophobic state (Lahann et al., 2003). Such a surface wetting switch may then be used to immobilize, for example, enzymes, as was discussed in the previous section. This is an example of switching both the orientation and the activity of adsorbed molecules.

Adsorbing proteins in the correct orientation on a surface is very relevant for immunoassays, in which antibodies are immobilized on a surface and used to detect the presence and concentration of specific antigens in a biological sample, but also for enzymatic microreactors, where the orientation (and folding state) of the enzyme determines its biocatalytic activity. Many reports have appeared in literature on the orientation of proteins on charged surfaces, both on theoretical and experimental work. Theoretical studies are based on two different types of models (Sheng et al., 2002): molecular models based on Molecular Dynamics or Monte Carlo simulations, which are very detailed at the atomic level but also very demanding in terms of computing power, and continuum models which treat proteins as colloidal particles with a (mostly uniform) charge distribution over its spherical surface and the

solvent as a continuum dielectric medium. A typical example of the latter is the Derjaguin–Landau–Verwey–Overbeek theory, which includes screened Coulombic repulsions and van der Waals attractions between proteins and surfaces. This theory describes most of the essential features of protein adsorption (see also the work of Roth et al. described in the previous section), but due to the assumption of a spherical protein with a charged shell inherently is unable to describe orientation effects. Therefore a compromise is often taken between the two types of models, by considering, for example, an immunoglobulin protein as a Y-shaped object with located charge centers on its branches and Monte Carlo modeling it at the mesoscopic scale (Sheng et al., 2002). In accordance with experimental data on oriented adsorption, Sheng et al. have shown that orientation of the adsorbed protein is based on a balance of van der Waals and electrostatic interactions. Van der Waals attraction leads to molecules lying flat on the surface, while in electrostatically dominated adsorption the orientation is determined by the dipole of the molecule which generally leads to alignment perpendicular to the surface. Experimental methods to probe protein orientation on charged surfaces are SIMS (Secondary Ion Mass Spectrometry) (Wang et al., 2004) and, more directly, atomic force microscopy (Wang et al., 2006). The latter work is particularly interesting because it reports that carbonic anhydrase is oriented with the majority of its active sites facing upward on a positively charged surface, and downward on a negatively charged surface, which shows that in principle the activity (or at least the accessibility of active sites on the enzyme) is controllable by the charge on the surface, which can be controlled by setting a specific voltage to the electrode.

An interesting effect of external electric fields on the selectivity of a homogeneous catalyst (an iron-oxo porphyrin compound) has recently been theoretically predicted (Shaik et al., 2004). The effect consists in changing the electronic structure of the catalyst in a field-direction-dependent manner. In doing so, the catalyst can be tuned either to epoxidation or to hydroxylation of propene. The electric field should be aligned along the SH–Fe–O axis of the molecule, which is in the direction perpendicular to the porphyrin ring. If the field is positive (i.e., pointing from S to O) the catalyst will acquire a thiolate radical character, therewith favoring the hydroxylation process by 6–10 $\mathrm{kcal\,mol^{-1}}$, while a negative field, turning the compound into a porphine radical cationic species, favors epoxidation by 2–6 $\mathrm{kcal\,mol^{-1}}$. Although a very interesting concept, experimental proof for the validity of this work has not yet been presented. An important issue to solve for practical evaluation of this idea is that one needs to fix the molecule in some way with respect to the electric field, for example, by immobilizing it on a surface, but in such a way that the porphyrin ring is still accessible from both sides and also with such a link to the surface that the activity is not affected. This is not an easy

problem to solve, and possibly the use of crystalline mesoporous materials like zeolites or MOFs may help, if a way is found to incorporate porphyrin-based catalysts in these materials in an ordered manner. We are not aware of any research in this direction.

Because of the current great interest in alternative energy in general and artificial photosynthesis in particular, and possible future developments of microreactors designed to perform photosynthesis, the following work is also worth mentioning. Protein-mediated electron transfer plays a key role in photosynthetic or metabolic reactions in living organisms, where such reactions generate electrons with a relatively low reduction potential. It has been established that several electron transfer reactions are rate limited by conformational changes at interfaces, for example, at a protein–protein interface or across an electrode–protein interface. In a study on cytochrome *c* which was electrostatically bound on Ag electrodes coated with a self-assembled monolayer of carboxyl-terminated alkylthiols the effect of the electric field strength on the activation energy of interfacial redox process was determined (Murgida and Hildebrandt, 2002). By varying the alkyl chain length and therewith the protein–electrode distance, the field strength was controlled. A high electric field increases the activation barrier for the structural reorganization of the protein, and rearrangement of the hydrogen bond network becomes the rate-limiting process in the interfacial redox process. It is concluded that this *electric-field-induced change in the activation barrier* which controls interfacial electron transfer dynamics in the case of cytochrome *c* might represent the modulation of biological charge-transfer dynamics at cell membranes. In a more recent publication (Kranich et al., 2008) two-color, time-resolved, surface-enhanced resonance Raman spectroelectrochemistry was used to monitor simultaneously and in real time the structure, electron-transfer kinetics, and configurational fluctuations of cytochrome *c* electrostatically adsorbed to electrodes in the same manner as described above. It is found that the interfacial electric field controls protein dynamics, which in turn control the overall electron transfer.

A controlled modification of the rate and selectivity of surface reactions on heterogeneous metal or metal oxide catalysts is a well-studied topic. Dopants and metal–support interactions have frequently been applied to improve catalytic performance. Studies on the *electric* control of catalytic activity, in which reactants were fed over a catalyst interfaced with O^{2-}-, Na^{+}-, or H^{+}-conducting solid electrolytes like yttrium-stabilized zirconia (or electronic–ionic conducting supports like TiO_2 and CeO_2), have led to the discovery of *non-Faradaic electrochemical modification of catalytic activity* (NEMCA, Stoukides and Vayenas, 1981), in which catalytic activity and selectivity were both found to depend strongly on the electric potential of the catalyst potential, with an increase in catalytic rate exceeding the rate expected on the basis of Faradaic ion flux by up to five orders of

magnitude (Vayenas et al., 1990). In a recent review (Vayenas and Koutsodontis, 2008), the current understanding of the mechanism and practical implications of NEMCA (or *electrochemical promotion*) have been discussed. It is important to note that short-circuiting catalyst and counter electrode (i.e., without external power source) is sufficient to induce NEMCA, which in that case is controlled by the spontaneous potential difference between catalyst and counter electrode due to their different activity for the catalytic reaction. Furthermore, if the support has mixed electronic and ionic conductivity (effectively giving an internal short circuit), like TiO_2, then NEMCA is induced even without external short circuit and therewith the system shows quite some similarity with the well-known metal–support interaction (Ertl et al.,1997; see also Figure 27c).

All the available experimental and theoretical work performed on NEMCA leads to the conclusion that electrochemical promotion is caused by electrocatalytic introduction of promoting species like O^{2-} or Na^+ from the solid electrolyte to the catalyst/gas interface where a double layer is formed, of which density and internal electric field vary with the applied potential. The latter affects the work function at the surface and therewith the bond strength of adsorbing reactants and intermediates. This causes the dramatic and reversible modification in catalytic rate (Vayenas and Koutsodontis, 2008; see Figure 28).

The mechanism behind the NEMCA effect (which is active in gases and at relatively high temperatures, of a few hundred degrees, where solid electrolytes have a significant conductivity) suggests that there may be another way of controlling activity on a catalyst particle, particularly in the liquid phase: the modification of the metal–support interaction by means of external fields. On may call this a *catalytic field-effect transistor* or *cat-FET* (although it is not used here as a transistor element). The hypothesis is that a field effect similar to that used in a transistor, may be used to control electronic depletion of a catalytic particle on an insulating support

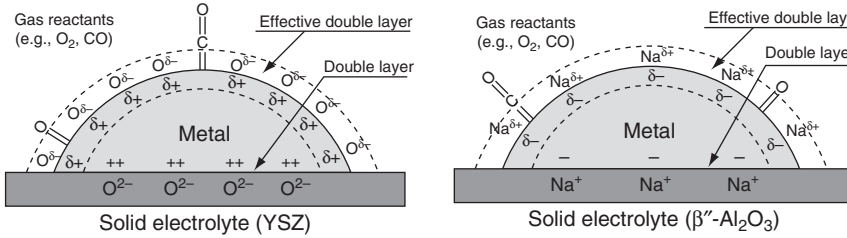

Figure 28 Metal electrode on O^{2-}-conducting (left) and Na^+-conducting (right) solid electrolyte. The figure depicts the metal–electrolyte double layer at the metal–gas interface due to electric potential-controlled ion migration, as well as its interaction with adsorbed reactants during CO oxidation (from Vayenas and Koutsodontis, 2008; reprinted with permission. Copyright 2008, American Institute of Physics).

material, and in that sense it relates to the metal–support interaction discussed earlier. The configuration envisioned is that of Figure 27c, but with a counter electrode at some distance from the metal particle, and an electrode on the backside of the support, to create an electric field over the particle–support interface. The idea relies on literature reports stating that the metal–support interaction on oxides involves a change in the electronic properties of the metal particle, correlated to the electron richness of the oxygen atoms in the support (Mojet et al., 1999), which is determined primarily by the ionic character of the cations in the oxide. In basic supports with alkaline cations, oxygen atoms are electron-rich, while they are electron poor on acidic supports. Density functional theory calculations for supported platinum particles furthermore revealed that for higher electron richness of the support oxygen atoms the complete Pt density of states shifts to higher energy, that is, lower binding energy, while the location of the interstitial bonding orbital moves from the metal–support interface to the surface of the Pt particle, and that the insulator-to-metal transition, which occurs with increasing Pt nanoparticle size, shifts to lower particle size on basic supports (Oudenhuijzen et al., 2004). The latter implies that the proposed field effect should be more proficient for smaller metal particles, where it also has to be taken into account that both the crystal habit (i.e., which crystal faces are present on the metal nanoparticle; this may be different on a different support; Somorjai et al., 2006) and the possible presence of oxygen (surface or subsurface; Schalow et al., 2006) on the particle may play a role.

Recent work demonstrates the feasibility of a somewhat similar concept as just described, based on a *semiconducting* SnO_2 catalyst, fabricated in the shape of a *nanowire*, and configured as FETs (Zhang et al., 2004b, 2005). The electron density in the nanowire was adjusted electrically, and in this way oxidation and reduction reactions at the surface of the SnO_2 wire could be modified by tuning the density of oxygen vacancies in the surface layer. This work is a very nice demonstration of the merger of different fields, that is, catalysis, nanotechnology, and microelectronics, and it would be quite feasible to combine this with microfluidics. It is quite possible that this is the direction in which the field of microreaction technology in future will develop.

6. CONCLUSION

In this chapter the use of electric fields as a means to control, activate, or modify chemistry in microreactor systems, and in some cases also in downstream work-up microsystems, was discussed. Particular attention was paid to microplasmas, in its many different configurations, because this is an upcoming field which allows us to perform chemistry at low

temperatures, which normally can only be performed at high temperatures, with possible advantages in energy efficiency. Novel configurations for plasma generation, based on nanostructured electrodes, were also highlighted. Special attention was also given to electrokinetic control of chemical reactions, a concept which only works efficiently in microsystems, because of the required localization of electric fields, and in some cases also the desired local high density of electric field lines. Electrokinetic concepts can be used to enhance or decrease fluid flow, or to transport and position or trap particles and molecules. A number of less known concepts (electric wind, electric swing adsorption, electrospray, and pulsed electric fields) were discussed, for which it remains to be seen if they will have relevance for microreaction technology. In the final section of this chapter some interesting principles to control the activity and orientation of adsorbed molecules, as well as the adsorption and desorption itself, were described. We predict that these principles will become very relevant in future microreaction technology, where the continuous progress in microsystems integration and in nanotechnology will allow us to combine new activation concepts with the beneficial high surface-to-volume ratio of microstructured systems to develop novel reactor and reaction concepts.

ACKNOWLEDGMENTS

The authors like to express their gratitude to the Technology Foundation STW, applied science division of NWO, and the technology program of the Ministry of Economic Affairs, The Netherlands, for financially supporting the project "Exciting chemistry in microreactors" (VICI "Vernieuwingsimpuls" program, project number 06626). J.G.E. Gardeniers also likes to thank the MESA + Research Institute for Nanotechnology for financial support of the SRO program "Mesofluidics."

REFERENCES

Ağiral, A., Eral, H.B., Mugele, F., and Gardeniers, J.G.E. unpublished results (2010).
Ağiral, A., and Gardeniers, J. G.E. *J. Phys. Chem. C* **112**, 15183 (2008a).
Ağiral, A., Groenland, A. W., Chinthaginjala, J. K., Seshan, K., Lefferts, L., and Gardeniers, J. G.E. *J. Phys. D: Appl. Phys.* **41**, 194009 (2008b).
Ağiral, A., Lefferts, L., and Gardeniers, J. G.E. *IEEE Trans. Plasma Sci.* **37**, 985 (2009).
Ağiral, A., Trionfetti, C., Lefferts, L., Seshan, K., and Gardeniers, J. G.E. *Chem. Eng. Technol.* **31**, 1116 (2008c).
Anderson, T. S., Ma, J. H., Park, S.-J., and Eden, J. G. *IEEE Trans. Plasma Sci.* **36**, 1250 (2008).
Astorga-Wells, J., Bergman, T., and Jörnvall, H. *Anal. Chem.* **76**, 2425 (2004).
Astorga-Wells, J., Vollmer, S., Tryggvason, S., Bergman, T., and Jörnvall, H. *Anal. Chem.* **77**, 7131 (2005).
Baba, K., Okada, T., Kaneko, T., and Hatakeyama, R. *Jpn. J. Appl. Phys.* **45**, 8286 (2006).
Baba, K., Okada, T., Kaneko, T., Hatakeyama, R., and Yoshiki, H. *Thin Solid Films* **515**, 4308 (2007).

Bak, E., Donten, M., Stojek, Z., and Scholz, F. *Electrochem. Commun.* **9**, 386 (2007).
Balint, I., and Aika, K.-I. *J. Chem. Soc., Faraday Trans.* **93**, 1797 (1997).
Banks, C. E., Davies, T. J., Evans, R. G., Hignett, G., Wain, A. J., Lawrence, N. S., Wadhawan, J. D., Marken, F., and Compton, R. G. *Phys. Chem. Chem. Phys.* **5**, 4093 (2003).
Bao, J., and Regnier, F. *J. Chromatogr.* **608**, 217 (1992).
Bazylak, A., Sinton, D., and Djilali, N. *J. Power Sources* **143**, 57 (2005).
Becker, K., Koutsospyros, A., Yin, S.-M., Christodoulatos, C., Abramzon, N., Joaquin, J. C., and Marino, G. B. *Plasma Phys. Control. Fusion* **47**, B513 (2005).
Becker, K. H., Kogelschatz, U., Schoenbach, K. H., Barker, R. (Eds.), Applications of atmospheric-pressure air plasmas, Chapter 9 *in* "Non Equilibrium Air Plasmas at Atmospheric Pressure". IOP Publ., Bristol, UK, 2004.
Becker, K. H., Schoenbach, K. H., and Eden, J. G. *J. Phys. D: Appl. Phys.* **39**, R55 (2006).
Belmont, C., and Girault, H. H. *Electrochim. Acta* **40**, 2505 (1995).
Beltrá, A. P., Bonete, P., González-García, J., García-García, V., and Montiel, V. *J. Electrochem. Soc.* **152**, D65 (2005).
Berge, B. *Comptes Rendus Acad. Sci., Ser. II* **317**, 157 (1993).
Blatter, F., Moreau, F., and Frei, H. *J. Phys. Chem.* **98**, 13403 (1994).
Block, J. *Z. Phys. Chem.* **39**, 169 (1963).
Bose, A. C., Shimizu, Y., Mariotti, D., Sasaki, T., Terashima, K., and Koshizaki, N. *Nanotechnology* **17**, 5976 (2006).
Bragg, A. E., Verlet, J. R.R., Kammrath, A., Cheshnovsky, O., and Neumark, D. M. *Science* **306**, 669 (2004).
Brown, B. D., Smith, C. G., and Rennie, A. R., *Phys. Rev. E* **63**, 016305 (2000).
Brusatori, M. A., Tie, Y., and Van Tassel, P. R., *Langmuir* **19**, 5089 (2003).
Bula, W.P.Microfluidic Devices for Kinetic Studies of Chemical Reactions, Ph.D. thesis, University of Twente (2009).
Burke, B. J., and Regnier, F. *Electrophoresis* **22**, 3744 (2001).
Chang, C.-C., and Yang, R.-J. *Phys. Fluids* **21**, 052004 (2009).
Chatterjee, A. N., and Aluru, N. R. *J. Microelectromech. Syst.* **14**, 81 (2005).
CHEMKIN. "Release 4.0 Software Package". Reaction Design, San Diego, CA (2004).
Chiang, W.-H., and Sankaran, R. M. *Appl. Phys. Lett.* **91**, 121503 (2007).
Chiang, W.-H., and Sankaran, R. M. *J. Phys. Chem. C* **112**, 17920 (2008).
Choi, J. O., Akinwande, A. I., and Smith, H. I. *J. Vac. Sci. Technol. B* **19**, 900 (2001).
Choudhary, T. V., Aksoylu, E., and Goodman, D. W. *Catal. Rev.* **45**, 151 (2003).
Cohen, A. E. *Phys. Rev. Lett.* **94**, 118102 (2005).
Cohen, A. E., and Moerner, W. E. *Appl. Phys. Lett.* **86**, 093109 (2005).
Cohen, A. E., and Moerner, W. E. *Proc. Natl. Acad. Sci.* **103**, 4362 (2006).
Collins, P. G., Arnold, M. S., and Avouris, Ph. *Science* **292**, 706 (2001).
Culbertson, C. T., and Jorgenson, J. W. *Anal. Chem.* **66**, 955 (1994).
Culbertson, C. T., and Jorgenson, J. W. *J. Microcolumn Sep.* **11**, 167 (1999).
Cummings, E. B., Griffiths, S. K., Nilson, R. H., and Paul, P. H. *Anal. Chem.* **72**, 2526 (2000).
De Jong, K. P., and Geus, J. W. *Catal. Rev. Sci. Eng.* **42**, 481 (2000).
De Malsche, W., Eghbali, H., Clicq, D., Vangelooven, J., Gardeniers, H., and Desmet, G. *Anal. Chem.* **79**, 5915 (2007).
De Malsche, W., Op De Beeck, J., Gardeniers, H., and Desmet, G. *J. Chromatogr. A* **1216**, 551 (2009).
Eijkel, J. C.T., Stoeri, H., and Manz, A. *Anal. Chem.* **71**, 2600 (1999).
Ertl, G., Knötzinger, H., and Weitcamp, J. "Handbook of Catalysis". Wiley VCH, Weinheim (1997).
Fletcher, P. D.I., Haswell, S. J., and Paunov, V. P. *Analyst* **124**, 1273 (1999).
Fletcher, P. D.I., Haswell, S. J., Pombo-Villar, E., Warrington, B. H., Watts, P., Wong, S. F.Y., and Zhang, X. *Tetrahedron* **58**, 4735 (2002).

Fletcher, P. D.I., Haswell, S. J., and Zhang, X. *Lab Chip* **2**, 115 (2001).
Foest, R., Schmidt, M., and Becker, K. *Int. J. Mass Spectrom.* **248**, 87 (2006).
Fowler, R. H., and Nordheim, L. *Proc. Roy. Soc. London A* **119**, 173 (1928).
Frei, H. *Science* **313**, 309 (2006).
Fridman, A. F. "Plasma Chemistry". Cambridge University Press, Cambridge (2008).
Garimella, S. V., and Liu, D. *J. Enhanced Heat Transfer* **16**, 237 (2009).
Ghanem, M. A., and Marken, F. *Electrochem. Commun.* **7**, 1333 (2005).
Go, D. B., Fisher, T. S., Garimella, S. V., and Bahadur, V. *Plasma Sources Sci. Technol.* **18**, 035004 (2009).
Go, D. B., Garimella, S. V., Fisher, T. S., and Mongia, R. K. *J. Appl. Phys.* **102**, 053302 (2007).
Grande, C. A., Ribeiro, R. P.P.L., and Rodrigues, A. E. *Energy Fuels* **23**, 2797 (2009).
Green, N. G., Ramos, A., González, A., Morgan, H., and Castellanos, A. *Phys. Rev. E* **61**, 4011 (2000).
Green, N. G., Ramos, A., González, A., Morgan, H., and Castellanos, A. *Phys. Rev. E* **66**, 026305 (2002).
Grotrian, W. *Ann. Physik* **47**, 141 (1915).
Grymonpré, D. R., Finney, W. C., Clark, R. J., and Locke, B. R. *Ind. Eng. Chem. Res.* **43**, 1975 (2004).
Gulder, O. L. *Energy Fuels* **23**, 591 (2009).
Günther, A., Khan, S. A., Thalmann, M., Trachsel, F., and Jensen, K. F. *Lab Chip* **4**, 278 (2004).
Hagelaar, G. J.M., and Pitchford, L. C. *Plasma Sources Sci. Technol.* **14**, 722 (2005).
Halpern, B., and Gomer, R. *J. Chem. Phys.* **51**, 1031 (1969).
Han, B., Li, Z., Pronkin, S., and Wandlowski, T. *Can. J. Chem.* **82**, 1481 (2004).
Harrison, D. J., Fluri, K, Seiler, K, Fan, Z., Effenhauser, C. S., Manz, A. *Science* **261**, 895 (1993).
Hartman, R. L., and Jensen, K. F. *Lab Chip* **9**, 2495 (2009).
Hessel, V., Hardt, S., and Löwe, H. "Chemical Microprocess Engineering. Fundamentals, Modelling and Reactions". Wiley VCH Verlag GmbH & Co. KGaA, Weinheim (2004).
Hessel, V., Renken, A., Schouten, J. C., and Yoshida, J. (Eds.) "Micro Process Engineering. A Comprehensive Handbook (3 volumes)". Wiley VCH Verlag GmbH & Co. KGaA, Weinheim (2009).
Horii, D., Amemiya, F., Fuchigami, T., and Atobe, M. *Chem. Eur. J.* **14**, 10382–10387 (2008).
Hsu, D. D., and Graves, D. B. *Plasma Chem. Plasma Proc.* **21**, 1 (2005).
Huber, D. L., Manginell, R. P., Samara, M. A., Kim, B.-I., and Bunker, B. C. *Science* **301**, 352 (2003).
Jähnisch, K., Hessel, V., Löwe, H., and Baerns, M. *Angew. Chem. Int. Ed.* **43**, 406 (2004).
Janev, R. K., and Reiter, D. *Phys. Plasmas* **11**, 780 (2004).
Jaworek, A., Krupa, A., and Czech, T., *J. Electrostat.* **65**, 133 (2007).
Jayashree, R. S., Gancs, L., Choban, E. R., Primak, A., Natarajan, D., Markoski, L. J., and Kenis, P. J.A. *J. Am. Chem. Soc.* **127**, 16758 (2005).
Jenkins, G., Franzke, J., and Manz, A. *Lab Chip* **5**, 711 (2005).
Jensen, K. F. *Chem. Eng. Sci.* **56**, 293 (2001).
Jiang, X. D., Li, R., Qiu, R., Hu, X., Liang, H. *Chem. Eng. J.* **116**, 149 (2006).
Jortner, J., and Kestner, N. R. (Eds.) "Electrons in Fluids". Springer Verlag, Berlin (1973).
Kadowaki, M., Yoshizawa, H., Mori, S., and Suzuki, M. *Thin Solid Films* **506**, 123 (2006).
Kalman, H., and Sher, E. *Appl. Therm. Eng.* **21**, 265 (2001).
Kane, C., and Tzédakis, T. *AIChE J.* **54**, 1365 (2008).
Kaniansky, D., Masár, M., Marák, J., and Bodor, R. *J. Chromatogr. A* **834**, 133 (1999).
Katayama, H., Honma, H., Nakagawara, N., and Yasuoka, K. *IEEE Trans. Plasma Sci.* **37**, 897 (2009).
Katsura, S., Harada, N., Maeda, Y., Komatsu, J., Matsuura, S.-I., Takashima, K., and Mizuno, A. *J. Biosci. Bioeng.* **98**, 293 (2004).

Kim, S.-O., and Eden, J. G. *IEEE Phot. Tech Lett.* **17**, 1543 (2005).
Kjeang, E., Djilali, N., and Sinton D. *J. Power Sources* **186**, 353 (2009).
Kogelschatz, U. *IEEE Trans. Plasma Sci.* **30**, 1400 (2002).
Kogelschatz, U. *Plasma Chem. Plasma Proc.* **23**, 1 (2003).
Kohlheyer, D., Besselink, G. A.J., Lammertink, R. G.H., Schlautmann, S., Unnikrishnan, S., Schasfoort, R. B.M. *Microfluid. Nanofluid.* **1**, 242 (2005).
Kohlrausch, F. *Ann. Phys. Chem. N. F.* **62**, 209 (1897).
Kolb, G., Hessel, V., Cominos, V., Hofmann, C., Löwe, H., Nikolaidis, G., Zapf, R., Ziogas, A., Delsman, E. R., de Croon, M. H.J.M., Schouten, J. C., de la Iglesia, O., Mallada, R., Santamaria, J. *Catal. Today* **120**, 2 (2007).
Kornienko, O., Reilly, P. T.A., Whitten, W. B., and Ramsey, J. M. *Anal. Chem.* **72**, 559 (2000).
Kranich, A., Ly, H. K., Hildebrandt, P., and Murgida, D. H. *J. Am. Chem. Soc.* **130**, 9844 (2008).
Kreuzer, H. J. *Surf. Interface Anal.* **36**, 372 (2004).
Krivenko, A. G., Komarova, N. S., Piven, N. P. *Electrochem. Commun.* **9**, 2364 (2007).
Krupke, R., Hennrich, F., Kappes, M. M., and Löhneysen, H. V. *Nano Lett.* **4**, 1395 (2004).
Krupke, R., Hennrich, F., von Löhneysen, H., and Kappes, M. M. *Science* **301**, 344 (2003).
Küpper, M., Hessel, V., Löwe, H., Stark, W., Kinkel, J., Michel, M., and Schmidt-Traub, H. *Electrochim. Acta* **48**, 2889 (2003).
Lahann, J., Mitragotri, S., Tran, T.-N., Kaido, H., Sundaram, J., Choi, I. S., Hoffer, S., Somorjai, G. A., Langer, R. *Science* **299**, 371 (2003).
Le Gac, S., and van den Berg, A. (Eds.) "Miniaturization and Mass Spectrometry". The Royal Society of Chemistry, Cambridge, UK (2009).
Lehr, W., and Hiller, W. *J. Electrostat.* **30**, 433 (1993).
Lei, L. C., Zhang, Y., Zhang, X. W., Du, Y. X., Dai, Q. Z., Han, S. *Ind. Eng. Chem. Res.* **46**, 5469 (2007).
Leonard, G. L., Mitchner, M., and Self, S. A. *J. Fluid Mech.* **127**, 123 (1983).
Lerner, E. J. *Industr. Phys.* **6**, 16 (2000).
Leroux, F., Campagne, C., Perwuelz, A., Gengembre, L. *J. Colloid Interf. Sci.* **328**, 412 (2008).
Leroux, F., Perwuelz, A., Campagne, C., and Behary, N. *J. Adhesion Sci. Technol.* **20**, 939 (2006).
Li, J.-R., Kuppler, R. J., and Zhou, H.-C. *Chem. Soc. Rev.* **38**, 1477 (2009).
Lieberman, M. A., and Lichtenberg, A. J. "Principles of Plasma Discharges and Materials Processing". John Wiley, New York (1994).
Locke, B., Sato, M., Sunka, P., Hoffmann, M., and Chang, J. *Ind. Eng. Chem. Res.* **45**, 882 (2006).
Luo, C.-P., Heeren, A., Henschel, W., and Kern, D. P. *Microelectr. Eng.* **83**, 1634 (2006).
MacDonald, S. M., Watkins, J. D., Bull, S. D., Davies, I. R., Gu, Y., Yunus, K., Fisher, A. C., Bulman Page, P. C., Chan, Y., Elliott, C., and Marken, F. *J. Phys. Org. Chem.* **22**, 52 (2009).
MacDonald, S. M., Watkins, J. D., Gu, Y., Yunus, K., Fisher, A. C., Shul, G., Opallo, M., and Marken, F. *Electrochem. Commun.* **9**, 2105 (2007).
MacInnes, J. M., Du, X., and Allen, R. W.K. *Trans. I. Chem. E, Part A.* **81**, Part A, 773 (2003).
Magnier, P., Hong, D. P., Leroy-Chesneau, A., Bauchire, J. M., and Hureau, J. *Exp. Fluids* **42**, 815 (2007).
Markarian, N., Yeksel, M., Khusid, B., and Farmer, K. *Appl. Phys. Lett.* **82**, 4839 (2003).
Marken, F., Webster, R. D., Bull, S. D., and Davies, S. G. *J. Electroanal. Chem.* **437**, 209 (1997).
McEwen, J.-S., and Gaspard, P. *J. Chem. Phys.* **125**, 214707 (2006) Magnier, P., Hong, D. P., Leroy-Chesneau, A., Bauchire, J. M., and Hureau, J. *Exp. Fluids* **42**, 815 (2007).
Meek, S. A., Conrad, H., and Meijer, G. *Science* **324**, 1699 (2009).
Melanson, J. E., Baryla, N. E., and Lucy, C. A. *Trans. Anal. Chem.* **20**, 365 (2001).
Michel, M., Schmidt-Traub, H., Ditz, R., Schulte, M., Kinkel, J., Stark, W., Küpper, M., and Vorbrodt, M. *J. Appl. Electrochem.* **33**, 939 (2003).
Mikkers, F. *Anal. Chem.* **71**, 522 (1999).
Millot, Y., Man, P. P., Springuel-Huet, M.-A., and Fraissard, J. *Comptes Rendus Acad. Sci. Ser. IIC Chem.* **4**, 815 (2001).

Min, S., Evrendilek, G. A., and Zhang, H. Q. *IEEE Trans. Plasma Sci.* **35**, 59 (2007).
Modi, A., Korathar, N., Lass, E., Wei, B., and Ajaya, P. M. *Nature* **424**, 171 (2003).
Mojet, B. L., Miller, J. T., Ramaker, D. E., and Koningsberger, D. C. *J. Catal.* **186**, 373 (1999).
Moon, H., Cho, S. K., Garrell, R. L., and Kim, C.-J. *J. Appl. Phys.* **92**, 4080 (2002).
Moon, S.-H., and Shim, J.-W. *J. Colloid Interf. Sci.* **298**, 523 (2006).
Moreau, E. *J. Phys. D: Appl. Phys.* **40**, 605 (2007).
Mori, S., Yamamoto, A., and Suzuki, M. *Plasma Sources Sci. Technol.* **15**, 609 (2006).
Mugele, F. *Soft Matter* **5**, 3377 (2009).
Mugele, F., and Baret, J.-C. *J. Phys. Condens. Matter* **17**, R705 (2005).
Mugele, F., Baret, J.-C., and Steinhauser, D. *Appl. Phys. Lett.* **88**, 204106 (2006).
Murgida, D. H., and Hildebrandt, P. *J. Phys. Chem. B* **106**, 12814 (2002).
Nenu, R. K.T., Yoshida, H., Fukui, K., and Yamamoto, T. *Powder Technol.* **196**, 147 (2009).
Nichols, K. F.P., and Gardeniers, H. J.G.E. *Anal. Chem.* **79**, 8699 (2007).
Nichols, K.P.F., and Gardeniers, H.J.G.E., Unpublished results (2006).
Niedziolka, J., Szot, K., Marken, F., and Opallo, M. *Electroanalysis* **19**, 155 (2007).
Nozaki, T., Hattori, A., and Okazaki, K. *Catal. Tod.* **98**, 607 (2004).
Nozaki, T., Sasaki, K., Ogino, T., Asahi, D., and Okazaki, K. *Nanotechnology* **18**, 235603 (2007a).
Nozaki, T., Sasaki, K., Ogino, T., Asahi, D., and Okazaki, K. *J. Therm. Sci. Technol.* **2**, 192 (2007b).
Oddy, M. H., Santiago, J. G., and Mikkelsen, J. C. *Anal. Chem.* **73**, 5822 (2001).
Oudenhuijzen, M. K., van Bokhoven, J. A., Ramaker, D. E., and Koningsberger, D. C. *J. Phys. Chem. B* **108**, 20247 (2004).
Paddon, C. A., Atobe, M., Fuchigami, T., He, P., Watts, P., Haswell, S. J., Pritchard, G. J., Bull, S. D., and Marken, F. *J. Appl. Electrochem.* **36**, 617 (2006).
Paik, P., Pamula, V. K., and Fair, R. B. *Lab Chip* **3**, 253 (2003).
Park, S-J., Kim, K. S., and Eden, J. G. *Appl. Phys. Lett.* **86**, 221501 (2005).
Paschen, F. *Ann. Phys.* **37**, 69 (1889).
Peng, H. Q., Alvarez, N. T., Kittrell, C., Hauge, R. H., and Schmidt, H. K. *J. Am. Chem. Soc.* **128**, 8396 (2006).
Pileni, M.-P. *Adv. Colloid Interf. Sci.* **46**, 139 (1993).
Pohl, H. A. "Dielectrophoresis. The Behavior of Neutral Matter in Non-Uniform Electric Fields". Cambridge University Press, Cambridge (1978).
Pollack, M. G., Shenderov, A. D., and Fair, R. B. *Lab Chip* **2**, 96 (2002).
Pompa, P. P., Bramanti, A., Maruccio, G., Cingolani, R., De Rienzo, F., Corni, S., Di Felice, R., and Rinaldi, R. *J. Chem. Phys.* **122**, 181102 (2005).
Pronkin, S., and Wandlowski, T. J. *Electroanal. Chem.* **550–551**, 131 (2003).
Qian, A., and Bau, H. H. *Anal. Chem.* **74**, 3616 (2002).
Qiao, Q, and Aluru, N. R. *J. Micromech. Microeng.* **12**, 625 (2002).
Raizer, Y. "Gas Discharge Physics". Springer Verlag, Heidelberg (1991).
Rayleigh, L. *Phil. Mag.* **14**, 184 (1882).
Rayner, D., Fietkau, N., Streeter, I., Marken, F., Buckley, B. R., Page, P. C.B., del Campo, J., Mas, R., Munoz, F. X., and Compton, R. G. *J. Phys. Chem. C* **111**, 9992 (2007).
Reuss, R. H., and Chalamala, B. R. *J. Vac. Sci. Technol. B* **21**, 1187 (2003).
Revermann, T., Götz, S., Künnemeyer, J., and Karst, U. *Analyst* **133**, 167 (2008).
Robinson, M. *Am. J. Phys.* **30**, 366 (1962).
Rode, S., and Lapicque, F. Microstructured reactors for electrochemical synthesis, Chapter 17 *in* "Micro Process Engineering. A Comprehensive Handbook. Volume 1, Fundamentals, Operations and Catalysis". Wiley VCH Verlag GmbH & Co. KGaA, Weinheim (2009).
Roth, C. M., Sader, J. E., and Lenhoff, A. M. *J. Colloid Interface Sci.* **203**, 219 (1998).
Ruthven, D. M., and Ching, C. B. *Chem. Eng. Sci.* **44**, 1011 (1989).
Salimi-Moosavi, H., Tang, T., and Harrison, D. J. *J. Am. Chem. Soc.* **119**, 8716 (1997).
Sankaran, R. M., Holunga, D., Flagan, R. C., and Giapis, K. P. *Nano Lett.* **5**, 537 (2005).

Schaffert, R. M. "Electrophotography". John Wiley and Sons, New York (1975).
Schalow, T., Brandt, B., Starr, D. E., Laurin, M., Shaikhutdinov, S. K., Schauermann, S., Libuda, J., and Freund, H.-J. *Angew. Chem. Int. Ed.* **45**, 3693 (2006).
Schasfoort, R. B.M., Schlautmann, S., Hendrikse, L., and van den Berg, A. *Science* **286**, 942 (1999).
Schoenbach, K. H., Moselhy, M., Shi, W., and Bentley, R. *J. Vac. Sci. Technol. A* **21**, 1260 (2003).
Schoenbach, K. H., Verhappen, R., Tessnow, T., Peterkin, P. F., and Byszewski, W. *Appl. Phys. Lett.* **68**, 13 (1996).
Scholz, F., Schröder, U., and Gulaboski, R. "Electrochemistry of Immobilized Particles and Droplets". Springer, Berlin (2005).
Schultz, Z. D., and Gewirth, A. A. *Anal. Chem.* **77**, 7373 (2005).
Sekiguchi, H., Ando, M., and Kojima, H. *J. Phys. D: Appl. Phys.* **38**, 1722 (2005).
Seto, T., Kwon, S.-B., Hirasawa, M., and Yabe, A. *Jpn. J. Appl. Phys.* **44**, 5206 (2005).
Shaik, S., de Visser, S. P., and Kumar, D. *J. Am. Chem. Soc.* **126**, 11746 (2004).
Sheldon, R. A. *Adv. Synth. Catal.* **349**, 1289 (2007).
Sheng, Y.-J., Tsao, H.-K., Zhou, J., and Jiang, S. *Phys. Rev. E* **66**, 011911 (2002).
Shimizu, Y., Sasaki, T., Ito, T., Terashima, K., and Koshizaki, N. *J. Phys. D: Appl. Phys.* **36**, 2940 (2003).
Shimizu, Y., Sasaki, T., Liang, C., Bose, A. C., Ito, T., Terashima, K., and Koshizaki, N. *Chem. Vap. Dep.* **11**, 244 (2005).
Shin, D. H., Kim, J.-E., Shim, H. C., Song, J.-W., Yoon, J.-H., Kim, J., Jeong, S., Kang, J., Baik, S., and Han, C.-S. *Nano Lett.* **8**, 4380 (2008).
Shiu, J.-Y, Kuo, C.-W., and Chen, P. *J. Am. Chem. Soc.* **126**, 8096 (2004).
Shrimpton, J. S., and Crane, R. I. *Chem. Eng. Technol.* **24**, 9 (2001).
Sichler, P., Buttgenbach, S., Hibbe, L. B., Shrader, C., and Gericke, K.-H. *Chem. Eng. J.* **101**, 465 (2004).
Skelton, V., Greenway, G. M., Haswell, S. J., Styring, P., Morgan, D. O., Warrington, B., and Wong, S. Y.F. *Analyst* **126**, 7 (2001a).
Skelton, V., Greenway, G. M., Haswell, S. J., Styring, P., Morgan, D. O., Warrington, B., and Wong, S. Y.F. *Analyst* **126**, 11 (2001b).
Solomentsev, Y., Böhmer, M., and Anderson, J. L. *Langmuir* **13**, 6058 (1997).
Somorjai, G. A., Contreras, A. M., Montano, M., and Rioux, R. M. *Proc. Natl. Acad. Sci.* **103**, 10577 (2006).
Sparreboom, W., van den Berg, A., Eijkel, J. C.T. *Nat. Nanotechnol.* **4**, 713 (2009).
Spindt, C. A., Brodie, I., Humphrey, L., and Westerberg, E. R. *J. Appl. Phys.* **47**, 5248 (1976).
Staack, D., Farouk, B., Gutsol, A., and Fridman, A. *Plasma Sources Sci. Technol.* **14**, 700 (2005).
Stankiewicz, A. I., and Moulijn, J. A. *Chem. Eng. Progr.* **96**, 22 (2000).
Stark, R. H., and Schoenbach, K. H. *J. Appl. Phys.* **85**, 2075 (1999).
Stoukides, M., and Vayenas, C. G. *J. Catal.* **70**, 137 (1981).
Studer, V., Pépin, A., Chen, Y., and Ajdari, A. *Microelectron. Eng.* **61–62**, 915 (2002).
Subramani, H. J., and Kurup, A. S. *Chem. Eng. J.* **120**, 169 (2006).
Suehiro, J., Hidaka, S.-I., Yamane, S., and Imasaka, K. *Sens. Act. B* **127**, 505 (2007).
Suga, S., Okajima, M., Fujiwara, K., and Yoshida, J.-I. *J. Am. Chem. Soc.* **123**, 7941 (2001).
Suzuki, M., Yasukawa, T., Mase, Y., Oyamatsu, D., Shiku, H., and Matsue, T. *Langmuir* **20**, 11005 (2004).
Tachibana, K. *IEEJ Trans. Electr. Electron. Eng.* **1**, 145 (2006).
Tang, C. S., Dusseiller, M., Makohliso, S., Heuschkel, M., Sharma, S., Keller, B., and Vörös, J. *Anal. Chem.* **78**, 711 (2006).
Taniguchi, T., Torii, T., and Higuchi, T. *Lab Chip* **2**, 19 (2002).
Tao, R., Huang, K., Tang, H., and Bell, D., *Energy Fuels* **22**, 3785 (2008).
Tao, R., Huang, K., Tang, H., and Bell, D. *Energy Fuels* **23**, 3339 (2009).
Tas, A., Plasma Induced Catalysis, Ph.D. dissertation, Technische Universiteit Eindhoven, The Netherlands (1995).

Teh, S. Y., Lin, R., Hung, L. H., Lee, A. P. *Lab Chip* **8**, 198 and 3604 (2008).
Thome, B., and Ivory, C. F. *J. Chromatogr. A* **953**, 263 (2002).
Thome, B., and Ivory, C. F. *J. Chromatogr. A* **1129**, 119 (2006).
Thome, B., and Ivory, C. F. *J. Chromatogr. A* **1138**, 291 (2007).
Townsend, J. S. *J. Franklin Inst.* **200**, 563 (1925).
Trau, M., Saville, D. A., Aksay, I. A. *Science* **272**, 706 (1996).
Trionfetti, C., Ağiral, A., Gardeniers, J. G.E., Lefferts, L., and Seshan, K. *ChemPhysChem* **9**, 533 (2008a).
Trionfetti, C., Ağiral, A., Gardeniers, J. G.E., Lefferts, L., and Seshan, K. *J. Phys. Chem. C* **112**, 4267 (2008b).
Trionfetti, C., Babich, I. V., Seshan, K., and Lefferts, L. *Appl. Catal. A* **310**, 105 (2006).
van der Wouden, E. J., Heuser, T., Hermes, D. C., Oosterbroek, R. E., Gardeniers, J. G.E., and van den Berg, A. *Colloids Surf. A* **267**, 110 (2005).
Van Krieken, M., and Buess-Herman, C. *Electrochim. Acta* **45**, 675 (1999).
Vayenas, C. G., Bebelis, S., and Ladas, S. *Nature* **343**, 625 (1990).
Vayenas, C. G., and Koutsodontis, C. *J. Chem. Phys.* **128**, 182506 (2008).
von Allmen, P., McCain, S. T., Ostrom, N. P., Vojak, B. A., Eden, J. G., Zenhausern, F., Jensen, C., and Oliver, M. *Appl. Phys Lett.* **82**, 2562 (2003).
von Engel, A. "Ionized Gases". Clarendon Press, Oxford (1955).
Wang, H., Castner, D. G., Ratner, B. D., and Jiang, S. *Langmuir* **20**, 1877 (2004).
Wang, J.-X., and Lunsford, J. H. *J. Phys. Chem.* **90**, 5883 (1986).
Wang, X., Zhou, D., Sinniah, K., Clarke, C., Birch, L., Li, H., Rayment, T., and Abell, C. *Langmuir* **22**, 887 (2006).
Watts, P., Haswell, S. J., Pombo-Villar, E. *Chem. Eng. J.* **101**, 237 (2004).
Wheeler, A. R., Moon, H., Kim, C.-J., Loo, J. A., and Garrell, R. L. *Anal. Chem.* **76**, 4833 (2004).
Wong, P. K., Chen, C.-Y., Wang, T.-H., and Ho, C.-M. *Anal. Chem.* **76**, 6908 (2004).
Yamatake, A., Fletcher, J., Yasuoka, K., and Ishii, S. *IEEE Trans. Plasma Sci.* **34**, 1375 (2006).
Yan, K., Li, R., Zhu, T., Zhang, H., Hu, X., Jiang, X., Liang, H., Qiu, R., and Wang, Y. *Chem. Eng. J.* **116**, 139 (2006).
Yang, Q., and Zhong, C. *ChemPhysChem* **7**, 1417 (2006).
Yoon, J.-Y., and Garrell, R. L. *Anal. Chem.* **75**, 5097 (2003).
Yoon, S. K., Choban, E. R., Kane, C., Tzedakis, T., and Kenis, P. J.A. *J. Am. Chem. Soc.* **127**, 10466 (2005).
Yoon, S. K., Fichtl, G. W., and Kenis, P. J.A. *Lab Chip* **6**, 1516 (2006).
Yoshida, J.-I. "Flash Chemistry. Fast Organic Synthesis in Microsystems". John Wiley & Sons, Ltd., Chichester (2008).
Yoshida, J.-I., Kataoka, K., Horcajada, R., and Nagaki, A. *Chem. Rev.* **108**, 2265 (2008).
Yoshitake, H., and Iwasawa, Y. *J. Phys. Chem.* **96**, 1329 (1992).
Zeng, X. A., Yu, S. J., Zhang, L., and Chen, X. D. *Innov. Food Sci. Emerging Technol.* **9**, 463 (2008).
Zhang, W., Fisher, T. S., and Garimella, S. V. *J. Appl. Phys.* **96**, 6066 (2004a).
Zhang, Y., Kolmakov, A., Chretien, S., Metiu, H., and Moskovits, M. *Nano Lett.* **4**, 403 (2004b).
Zhang, Y., Kolmakov, A., Lilach, Y., and Moskovits, M. *J. Phys. Chem. B.* **109**, 1923 (2005).
Zhao, Y., and Cho, S. K. *Lab Chip* **7**, 273 (2007).